

THESIS FOR THE DEGREE OF DOCTOR OF PHILOSOPHY IN THERMO AND  
FLUID DYNAMICS

Active Flow Control for Reducing Drag on Trucks: from  
Concept to Full Scale Testing

GUGLIELMO MINELLI

Department of Mechanics and Maritime Sciences  
CHALMERS UNIVERSITY OF TECHNOLOGY

Göteborg, Sweden 2017

Active Flow Control for Reducing Drag on Trucks: from Concept to Full Scale Testing  
GUGLIELMO MINELLI

© GUGLIELMO MINELLI, 2017

Doktorsavhandlingar vid Chalmers tekniska högskola

Ny serie nr. 4343

ISSN 0346-718X

Department of Mechanics and Maritime Sciences

Chalmers University of Technology

SE-412 96 Göteborg

Sweden

Telephone: +46 (0)31-772 1000

Active Flow Control for Reducing Drag on Trucks: from Concept to Full Scale Testing  
Thesis for the degree of Doctor of Philosophy in Thermo and Fluid Dynamics  
GUGLIELMO MINELLI  
Department of Mechanics and Maritime Sciences  
Chalmers University of Technology

## ABSTRACT

There is no doubt that road vehicle transportation is needed to improve efficiency, to reduce power consumption and to contribute to a sustainable mobility. Aerodynamics plays a crucial role in this, and its optimization can have a significant impact on fuel efficiency. The work reported in this thesis thus investigates the applicability of an active flow control technique able to improve the aerodynamic performance of trucks.

CFD simulations and wind tunnel experiments are conducted to explore the potential of such a device. The process starts with a preliminary LES study ( $Re = 1 \times 10^5$ ) and ends with a proof of concept full scale test of a real truck ( $Re = 3.5 \times 10^6$ ). The PANS method and scaled model wind tunnel experiments were essential to bridge the initial preliminary findings to the final full scale test. PANS was first validated (using in-house experimental data and data from test cases) and then used to simulate the efficacy of AFC at higher  $Re$  ( $Re = 5 \times 10^5$ ), introducing realistic flow conditions (wind gusts). In addition, wind tunnel experiments of a scaled, simplified truck cabin were used to demonstrate the applicability of flow control.

The results focus on two main points. First, synthetic jets were shown to be an effective and low energy consumption technique to control a pressure induced separated flow and for reducing drag on trucks. Second, PANS was shown to be an interesting method for industrial applications. Its capability to resolve unsteady flow cases preserving the accuracy of the flow structures prediction is shown, even when meshes are relatively coarse.

Keywords: Vehicle Aerodynamics, Active Flow Control, AFC, Large Eddy Simulations, LES, Partially-Averaged Navier-Stokes, PANS, Experiments, Wind Tunnel, PIV, Proper Orthogonal Decomposition, POD



## LIST OF PUBLICATIONS

This thesis consists of an extended summary and the following appended papers. Papers A-D are published in scientific journals. Paper E is currently under review for journal publication. Paper F is accepted for conference presentation.

- Paper A** G. Minelli, S. Krajnović, B. Basara, B. R. Noack, "Numerical Investigation of Active Flow Control Around a Generic Truck A-pillar" in *Flow, Turbulence and Combustion*. Vol. 97, 1235-1254, 2016
- Paper B** G. Minelli, A. Hartono, V. Chernoray, L. Hjelm, S. Krajnović, "Aerodynamic Flow Control for a Generic Truck Cabin Using Synthetic Jets" in *Wind Engineering and Industrial Aerodynamics*. Vol. 168, 81-90, 2017
- Paper C** S. Krajnović, G. Minelli, B. Basara "Partially-averaged Navier–Stokes simulations of Two Bluff Body Flows" in *Applied Mathematics and computation* Vol. 272, 692-706, 2016
- Paper D** G. Minelli, A. Hartono, V. Chernoray, L. Hjelm, B. Basara, S. Krajnović, "Validation of PANS and Active Flow Control for a Generic Truck Cabin" in *Wind Engineering and Industrial Aerodynamics* Vol. 171, 148-160, 2017.
- Paper E** G. Minelli, S. Krajnović, B. Basara, "A Flow Control Study of a Simplified, Oscillating Truck Cabin using PANS" in *Journal of Fluid Engineering*. Under review
- Paper F** G. Minelli, A. Hartono, V. Chernoray, L. Hjelm, B. Basara, S. Krajnović, "Development of Active Flow Control for Trucks" in the *3rd Thermal and Fluids Engineering Conference (TFEC)*, March 4–7, 2018, Fort Lauderdale, FL, USA



## OTHER RELEVANT PUBLICATIONS

- Publication I** S. Krajnovic, G. Minelli "Status of PANS for bluff body aerodynamics of engineering relevance" in *Progress in Hybrid RANS-LES Modelling: Papers Contributed to the 5th Symposium on Hybrid RANS-LES Methods*, 19-21 March 2014, College Station, A&M University, Texas, USA, 2015
- Publication II** G. Minelli, S. Krajnovic "Numerical Investigation of the Actuated Flow on a Bluff Body" in the *5th International Conference on Jets, Wakes and Separated Flows, ICJWSF2015*, Stockholm, Sweden, 15-18 June 2015. 185 p. 295-302
- Publication III** G. Minelli, S. Krajnovic, B. Basara "Actuation of the flow field around a frontstep with a rounded leading edge" in the *8th international symposium on Turbulence, Heat and Mass Transfer*, September 15-18, 2015, Sarajevo, Bosnia and Herzegovina
- Publication IV** G. Minelli, A. Hartono, V. Chernoray, L. Hjelm, B. Basara, S. Krajnović "Experimental and Numerical Investigation of Active Flow Control on a Generic Truck Cabin" in the *11th International ERCOFTAC Symposium on Engineering Turbulence Modelling and Measurements*, September 21-23, 2016, Palermo, Italy
- Publication V** G. Minelli, S. Krajnović, B. Basara "Partially-Averaged Navier-Stokes Simulations of Flows Around Generic Vehicle at Yaw" in the *SAE Technical Papers: SAE 2016 World Congress and Exhibition*, Detroit, United States, 12-14 April 2016
- Publication VI** G. Minelli, A. Hartono, V. Chernoray, L. Hjelm, B. Basara, S. Krajnović "PANS Validation and Active Flow Control for a Simplified Truck Cabin" in the *16th European Turbulence Conference*, 21-24 August, 2017, Stockholm, Sweden.
- Publication VII** G. Minelli, A. Hartono, V. Chernoray, L. Hjelm, S. Krajnović, "Flow Control for a Generic Truck Cabin Using Synthetic Jet" in the *European Drag Reduction and Flow Control Meeting-EDRFCM 2017*, April 3-6, 2017, Rome, Italy
- Publication VIII** G. Minelli, B. Basara, S. Krajnović "PANS Study of the Flow around an Oscillating, Simplified Truck Cabin with Flow Control" in the *Proceedings of the ASME 2017 Fluids Engineering Division Summer Meeting FEDSM2017*, July 30-August 3, 2017, Waikoloa, USA
- Publication IX** G. Minelli, B. Basara, S. Krajnović "A LES study on the Effect of Periodic Gusts on a Truck Model" in the *International Conference on Jets, Wakes and Separated Flows, ICJWSF-2017*, 9-12 October 2017, Cincinnati, Ohio, USA

**Publication X**

A. Rao, G. Minelli, B. Basara and S. Krajnović "On the two flow states in the wake of a hatchback Ahmed body" in *Wind Engineering and Industrial Aerodynamics*, 2017, in print.

## ACKNOWLEDGEMENTS

I want to express my gratitude to my advisor, Prof. Siniša Krajnović, who gave me the opportunity to work at this project. Siniša, thank you for your constant support which formed my knowledge and my attitude in research. Thank you for every brilliant discussion which helped me to step further, and thank you for all the trust you put in me since the first time we met.

I am grateful to Linus Hjelm, Björn Berqvist and the Volvo Trucks team for all support and guidance received, for encouraging the experimental part of the project and for letting me be part of the team in Canada. Thanks to associate Prof. Chernoray and Erwin Adi Hartono for being so ready to transfer knowledge and experience in the lab. Many thanks go to Prof. Basara for solving any doubts regarding AVL Fire and freely sharing his "numerical knowledge". His contribution to the project was doubtless key. I want also to acknowledge Prof. Noack for sharing his knowledge and introducing me to modal analysis. Thank you Prof. Keirsbulck, Camila and David, for hosting me in Valenciennes and giving me the opportunity to collaborate with you.

Thanks also to my former colleagues Eysteinn and Jan for being so helpful during my first year of Ph.D., to Daniel for all funny episodes of the everyday office life and to Lars, for being the solid rudder of the ship (a reference to maritime science was necessary). I am extremely thankful to all my colleagues/friends at the division of fluid dynamic and combustion. Thank you to contribute to an inspiring work environment and to an enjoyable life outside the office.

I am really thankful I had the chance to meet a beautiful "family" here in Göteborg and I am proud to have friends that always strive to keep our relationship going strong despite the distance.

I am really grateful to my family (Anna, Daniela and Laura), for being such great friends, advisers and supporters in all decisions I take.

Last but not least, I want to thank my wonderful wife Rita. There are no words to describe how full of joy is my life with you, "You light up my days".

This work is funded by the Swedish Energy Agency and supported by Volvo Trucks. Software licenses were provided by AVL List GMBH. Computations were performed at SNIC (Swedish National Infrastructure for Computing) at the Center for Scientific Computing at Chalmers (C3SE) and the National Supercomputer Center (NSC) at LiU.



*To my father, who shaped my soul without being here*



# Contents

<b>Abstract</b>	<b>i</b>
<b>List of publications</b>	<b>iii</b>
<b>Other relevant publications</b>	<b>v</b>
<b>Acknowledgements</b>	<b>vii</b>
<b>I Extended Summary</b>	<b>1</b>
<b>1 Introduction</b>	<b>1</b>
1.1 Scope and objective . . . . .	2
<b>2 Flow control for aerodynamic drag reduction</b>	<b>3</b>
2.1 Heavy vehicle aerodynamics, in short . . . . .	3
2.2 Flow control . . . . .	5
2.3 Active flow control at the A-pillar of a truck . . . . .	7
<b>3 Computational fluid dynamics for turbulent flows</b>	<b>9</b>
3.1 From DNS to RANS. Accuracy and efficiency . . . . .	9
3.2 Large eddy simulation and bridging methods . . . . .	11
3.2.1 The LES equations . . . . .	13
3.2.2 PANS $k - \varepsilon - \zeta - f$ . . . . .	14
3.2.3 Numerical schemes . . . . .	16
<b>4 Experiments and wind tunnels</b>	<b>17</b>
4.1 Measurement techniques . . . . .	17
<b>5 Modal decomposition</b>	<b>19</b>
<b>6 The work flow</b>	<b>21</b>
6.1 Phase 1: preliminary LES on flow control . . . . .	22
6.2 Phase 2: experiments on flow control . . . . .	22
6.3 Phase 3: PANS validation . . . . .	24
6.4 Phase 4: PANS for an oscillating cabin . . . . .	24

6.5	Phase 5: full scale test (unpublished results) . . . . .	25
6.6	Phase 6: microblowers for AFC (unpublished results) . . . . .	28
<b>7</b>	<b>Summary of Papers</b>	<b>31</b>
7.1	Paper A . . . . .	31
7.2	Paper B . . . . .	31
7.3	Paper C . . . . .	32
7.4	Paper D . . . . .	33
7.5	Paper E . . . . .	33
7.6	Paper F . . . . .	34
<b>8</b>	<b>Conclusion and Future Directions</b>	<b>37</b>
	<b>References</b>	<b>38</b>
<b>II</b>	<b>Appended Papers A–F</b>	<b>45</b>

# Part I

## Extended Summary

### 1 Introduction

Mobility is the ability to move freely and easily (Oxford dictionary). This is a simple definition that describes our future world vision. It feels good to be a part of our planet and even better to have potential access to every part of our world. The evolution of mobility has enlarged our vision, expanded our culture, answered our needs and, not least, satisfied our dreams and desires. Transportation has evolved into the new frontier of technological breakthroughs affecting and improving our daily private and work life. Cars and trucks enter actively or passively into our routine, and they have raised our standard of living. At this point, we do not want to settle for less, and this is why we need to preserve our mobility, developing transportation in a larger context of a sustainable future. The world has started to take serious actions to develop sustainable mobility in 2015. The Paris agreement set ambitious standards for emission reduction (and zero emission vision), achievable only by taking drastic decisions in the transport sector. In fact, at present, transportation accounts for almost a quarter of the total greenhouse gas (GHG) emissions (Fig. 1) and it is the main cause of air pollution in cities. *The ambition is clear: by mid-century, greenhouse gas emissions from transport will need to be at least 60% lower than in 1990 and be firmly on the path towards zero. Emissions of air pollutants from transport that harm our health need to be drastically reduced without delay [1].*

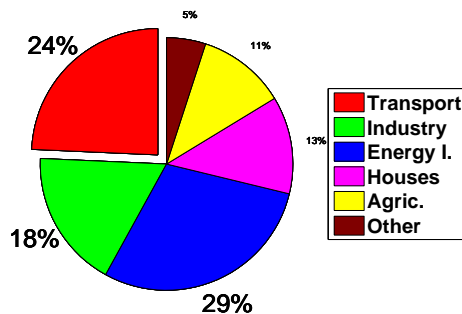


Figure 1: *The GHG emissions share.*

The ground transportation industry is also finally taking drastic decisions to converge toward this common goal. Trucks in particular, need to improve their efficiency to extend their mileage and decrease their power consumption. But, the final goal is still far away. Thus, improving the aerodynamic features of heavy trucks and road vehicles is a necessary contribution toward the target.

## 1.1 Scope and objective

This thesis focuses on the aerodynamic study of an active flow control (AFC) technique, applied to heavy ground vehicles. Computational fluid dynamics (CFD) and wind tunnel (WT) experiments are the engineering tools used to investigate and analyze the AFC effects on the aerodynamic performance. The overall goal was to verify and implement an AFC in a real truck cabin. This work was divided into six phases that led to the final proof of concept on a full scale model:

- In phases 1 and 2 the effectiveness of the AFC was proven numerically and experimentally.
- In phases 3 and 4 an alternative CFD tool (partially averaged Navier-Stokes PANS) was first validated (phase 3) and later used to simulate the robustness of the AFC when more realistic flow conditions (higher Reynolds number and wind gusts) were applied.
- In phase 5 the aerodynamic benefits of the AFC were measured on a full scale truck model.
- The last, and ongoing, phase 6 aims to find alternative and more efficient AFC devices for a large scale implementation.

The appended papers provide details on the methods used and outcomes. However, the following chapters summarize the basic principles of heavy vehicle aerodynamics and the engineering tools used in the thesis. In conclusion, chapter 6 aims to frame the chronological process and chapter 7 provides a summary of the appended papers. Conclusions and future developments are presented in chapter 8.

## 2 Flow control for aerodynamic drag reduction

Higher efficiency is achieved by minimizing aerodynamic drag and drag is reduced by controlling the flow surrounding a vehicle. This chapter helps the reader to become familiar with external vehicle aerodynamics and the principles behind flow control.

### 2.1 Heavy vehicle aerodynamics, in short

To understand the need for higher aerodynamic performance of trucks, it is necessary to break down transportation power consumption into air, maritime and road mobility, Fig. 2a. Road vehicles, in general, accounts for more than 70% of the total transport power consumption, being by far the biggest producer of GHG emissions. Aerodynamic drag is defined as the fluid drag force that acts on any moving solid body in the direction of the fluid free-stream flow [2] and more than 60% of the total power generated by a road vehicle is needed to overcome drag, Fig. 2b. For example, with a medium size car moving at 100 km/h or a semi-truck moving at cruise speed (80 km/h), drag accounts for 80-60% of the total resistance of motion.

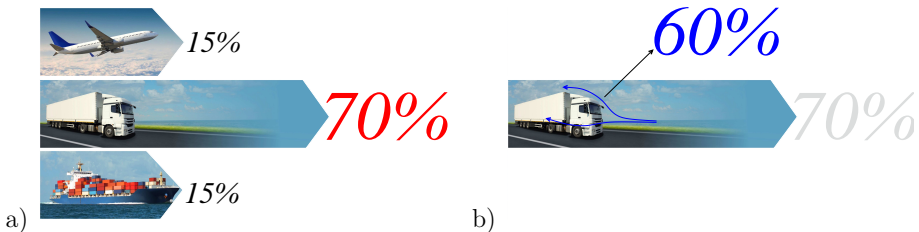


Figure 2: a) *The share of power consumption in transportation.* b) *The impact of drag on power consumption.*

In fact, the aerodynamic drag  $D$  increases with the square of the vehicle speed  $U_{inf}$ . For this reason,  $D$  remains the focal point of vehicle aerodynamics, whether the objective is the efficiency or the performance. The complete relation between  $D$  and  $U_{inf}$  is:

$$D = C_d A \frac{\rho}{2} U_{inf}^2. \quad (1)$$

Therefore,  $D$  is determined by the shape of the model, described by the aerodynamic coefficient  $C_d$ , and its frontal area  $A$  (Fig. 3), while the density  $\rho$  is a characteristic of the external flow.

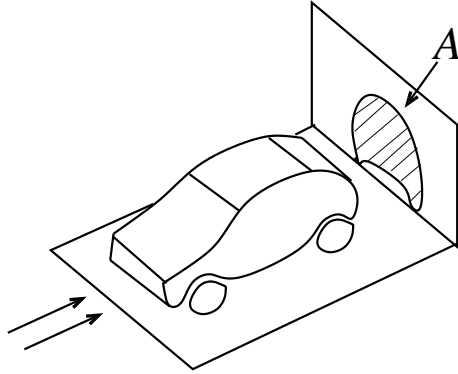


Figure 3: *The projected area A.*

At this point, it is important to distinguish between streamlined and bluff bodies. A streamlined body produces a thin wake which confers a low value of drag, Fig. 4a. On the other hand, when the body's wake is comparable to its characteristic dimension, it is generally called a bluff body, Fig. 4b. All road vehicles and heavy trucks are classified as bluff bodies. They produce a large wake, and they experience separated flow on large areas of their external surface.

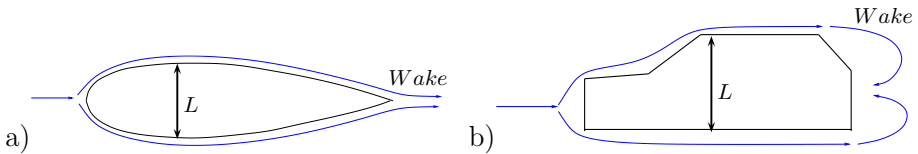


Figure 4: *a) A streamlined body. b) A bluff body.*

In particular, every time the flow detaches from the surface of the vehicle (blue lines in Fig. 5), the  $C_d$  increases. More specifically, the main sources of drag for a heavy truck, principally arise from four different regions [3]: the wake region, wheel housings and underbody [4,5], the gap between the tractor and the trailer and the front of the tractor, Fig 5.

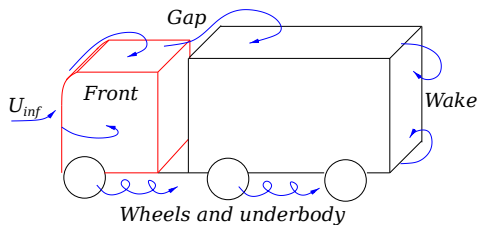


Figure 5: *Main sources of aerodynamic drag.*

The role of aerodynamic research is to investigate solutions to improve the aerodynamic performance of these regions. The main objective is therefore to reduce drag, manipulating or better put, controlling the flow to a more desired state, ideally suppressing any separated flow area. This type of practice is called flow control, and comprehends several different techniques that have different advantages and drawbacks.

## 2.2 Flow control

Following the words of Gad-El-Hak [6], flow control is “the attempt to favourably alter the character or disposition of a flow field that is of concern.” One of the first human empirical attempts for a favourable flow control can be found in the fin-stabilizer of arrows. Empirical attempts bring practice slowly to science, and the science of flow control started in 1904, when the boundary layer theory and the scientific method of flow control was introduced by Prandtl [7]. The economic crisis and wars during the 20<sup>th</sup> century pushed forward every scientific field, faster than in any other century before. The science of flow control was not an exception. The newborn aeronautic field was the natural expression of this science and during the years, new methodologies were discovered to overcome challenges and open new possibilities. The challenge of today is to extensively bring flow control to civil transport, extending aeronautic solutions to all forms of commercial transport, e.g. passenger cars, trains and trucks. When comes to trucks, the challenge is amplified by the restrictions made by design regulations. A truck is indeed designed for cargo and stocking operations, distancing its shape from being aerodynamically efficient. Therefore, the main challenge consists in keeping the cargo-optimized shape, minimizing the aerodynamic drag. The first part of the 20<sup>th</sup> century has observed a massive development of the road transportation industry that did not take into account the potential of an optimized aero design. Starting in the late 1970s with the advent of the oil crisis, extensive aerodynamic research was performed and still continues on heavy vehicles [8, 9]. This period has seen the evolution of several devices, add-ons and design alterations applied to trucks. For example, in the early 1980s the front corners of the tractor were smoothed to rounded and flaps bridging the gap between the tractor and the trailer are extensively used today. Flaps applied at the trailing edge [10, 11], flow treatment devices for the underbody [12] or the trailer base [13], cavities and side skirts [14–16], boat tails [17] and other add-ons [18] have recently been investigated in order to delay flow separation, thus reducing the wake effect. Such techniques have tried to reduce drag with various success, but they all have a common drawback: they are passive flow control techniques, thus designed to work at a nominal condition, which rarely matches the real operating flow state. Here rises the importance of designing a flow control which is adaptable to the flow condition, an AFC (reviews are provided in [6, 19, 20]). AFC opens the possibility for feedback control (closed-loop) once the open-loop flow mechanisms are well understood. The main idea behind AFC is to directly interact with the turbulent boundary layer in order to delay the separation of the flow from a solid surface. In other words, a fluid flow in presence of an adverse pressure gradient (from point *A* to point *B* in Fig. 6) loses kinetic energy and tends to depart from the solid surface creating a recirculation bubble of separated

flow [21, 22], Fig. 6. Bearing this in mind, introducing an AFC between points  $A$  and  $B$  in Fig. 6, it is possible to delay and even suppress the separated region.

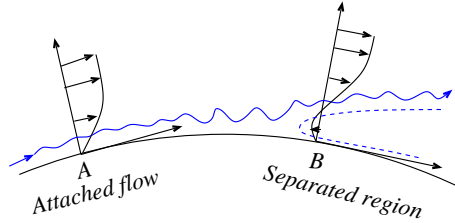


Figure 6: *Turbulent boundary layer separation. The solid blue line represents the incoming flow, while the dashed blue line represents the region of the mean reverse flow due to separation.*

In general, AFC can be classified into three main categories. The first one is flow control by means of moving surfaces (for example moving cylinders [23–26]). This is achieved by the motion of parts of the body surface in order to energize the turbulent boundary layer shown in Fig. 6. The main disadvantage of this technique lies in its applicability; it requires mechanical transmission and electric engines, which are not easy to embed for example in a vehicle geometry. AFC can also be introduced by means of steady or pulsating jets [27–30] where a jet flow is introduced before the flow separation. In this case a stream of one fluid mixes with the surrounding medium (external air), but it requires for example an air pump and a tank to store the pressurized first fluid. The third methodology can be categorized under the name of synthetic jets. The latter technique has now gained much interest in different fields (from thermal management to flow control of aerofoils) thanks to its versatility. It is a type of jet flow defined by zero net mass flux (ZNMF) and this jet is "synthesized" from the surrounding fluid [31]. A synthetic jet flow can be created by plasma actuation or by means of the time periodic motion of a flexible diaphragm in a sealed cavity, Fig. 7. Plasma actuator research for flow control started 20 years ago [32] and produced promising results (reviews are provided in [33–36]), yet are far from being extensively applicable in the near future. Using very high voltages, plasma actuators are able to produce an electric wind (a synthetic jet) synthesized from the surrounding flow. Nevertheless, more research is needed to understand, for example, the degradation of the actuation over time and to optimize their power consumption [37]. Thus, a synthetic jet produced by a flexible diaphragm turned out to be one of the most effective ways to manipulate the flow field. This technique allows much lower power consumption and an easier implementation, as compared to plasma actuators. Promising results of this technique were found in several studies, for both aerofoils [38–41], bluff bodies [42, 43] and generic vehicles [44]. Fig. 7 shows a sketch of the working principle of such a device. Despite the former research, the implementation of flow control on real vehicles is still far off. Therefore, one of the objectives of this Ph.D. thesis is to bridge this gap, implementing such a concept in a real truck.

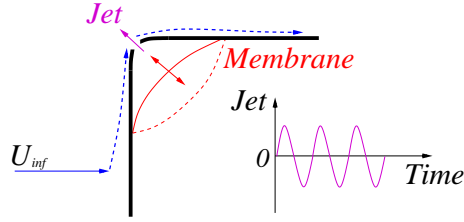


Figure 7: A jet flow synthesized by the time periodic motion of a flexible diaphragm in a sealed cavity. The dashed blue lines represent attached flow subjected to flow control.

## 2.3 Active flow control at the A-pillar of a truck

When a truck moves with a certain speed  $U_{inf}$ , the flow impinges the front section of the tractor and migrates toward the A-pillars. At this point, the flow separates creating a recirculation flow region which increases drag, Fig. 8. With rounded A-pillars, the aerodynamic of the truck cabin improves, to some extent, by mitigating the adverse pressure gradient. Cooper [8] describes the use of rounded corners, showing the effectiveness of this acknowledged expedient. Thus, the question that now emerges is: why do we still need to control the flow in this region? The answer is twofold. Normally the flow impinging the front is not oriented along the direction of the truck (even when the vehicle is moving at cruise speed), due to side wind, gusts, atmospheric turbulence or steering. In this situation the truck experiences an angle with respect to the direction of the flow [45–47]. This angle is generally called the yaw angle  $\beta$ . At cruise speed,  $\beta$  varies between  $5^\circ < \beta < 10^\circ$ , which is sufficient to induce the separation visualized in Fig. 8 and worsen the aerodynamic performance. The second aspect is that by using an AFC, the radius of the A-pillar can be decreased, gaining space inside the truck’s cabin yet still having the required aerodynamic performance.

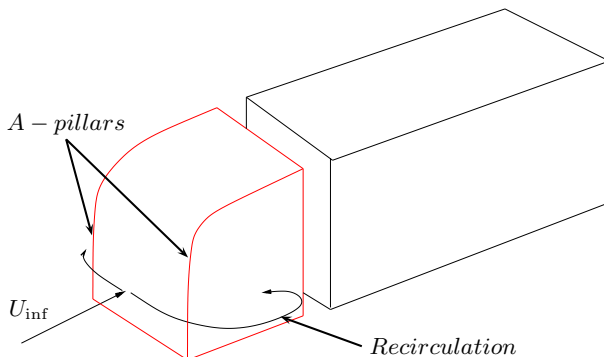


Figure 8: The flow recirculation bubble at the A-pillar.

The A-pillar separation can be reconnected, to some extent, to the flow behaviour visualized in leading-edge separation studies [48, 49] and stalled aerofoils [38, 50–52], Fig.

9. The main features that characterize the topology of this flow are the separated shear layer, the near/side wake shedding and their interaction. Figure 9b depicts a top view of a generic truck cabin and a flow topology similar to the one described by stalled aerofoils, Fig. 9a. The natural frequency of the shear layer is usually higher compared to the near wake shedding, but the coupling of them results in a collective interaction during the formation of the vortices [53].

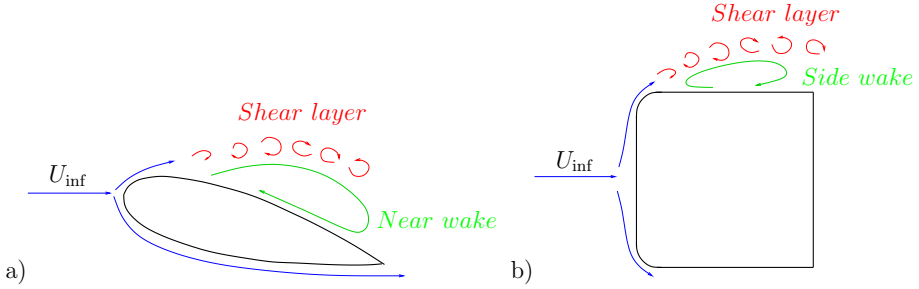


Figure 9: a) A stalled aerofoil flow topology. b) Top view of the separated flow topology at the A-pillar of a truck.

The structures present in the shear layer are smaller containing a smaller amount of energy, yet are dynamically important for the near/side wake formation. At this point, the AFC frequency of the flexible diaphragm becomes crucial to interact with the natural frequencies of the flow. The result of this interaction is an alteration of the surrounding flow field and a drastic change of the aerodynamic performance. The sketch presented in Fig. 10 shows the full potential of this AFC, ideally able to favourably affect the incipient A-pillar flow separation of a truck cabin. The study of such a turbulent flow requires particular numerical methods that are presented in the following section.

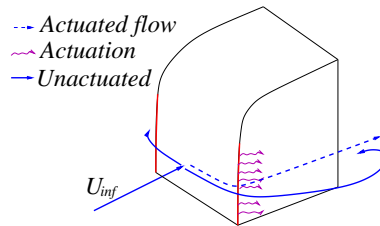


Figure 10: The potential of the actuation.

# 3 Computational fluid dynamics for turbulent flows

It is very common to observe turbulent flows in our everyday surroundings. From waterfalls to the smoke rising from a chimney, from the motion of sea waves to the flow around moving vehicles, and other engineering applications. There is no exact definition of turbulence but a turbulent flow has common and well defined characteristics:

- A turbulent flow is three dimensional.
- A turbulent flow is unsteady and contains high spatial and temporal fluctuations. The fluid velocity field varies significantly and irregularly in both position and time.
- A turbulent flow has the ability to mix and transport fluid more than a comparable laminar flow [54].
- A turbulent flow is dissipative, meaning that it loses part of its energy (kinetic energy) to internal energy (heat), through the cascade process, Fig. 11.
- As a consequence of the above, turbulence needs always to be sustained by additional kinetic energy.
- A turbulent flow is chaotic and unpredictable.

The difference between laminar and turbulent flows has been observed for centuries but only in 1894 did Reynolds define the characteristics of the transition between the two flow states, [55]. He also realized and experimented with the non dimensional parameter  $Re$  (Reynolds number) which defines the transition based on the flow (using a velocity scale  $\mathcal{U}$ ), the fluid (using the kinematic viscosity  $\nu$ ) and the geometry (using a length scale  $\mathcal{L}$ ),

$$Re = \frac{\mathcal{U}\mathcal{L}}{\nu} \tag{1}$$

$Re$  also represents the ratio between inertial and viscous forces. Thus, high- $Re$  turbulent flows are mainly characterized by inertial forces while the viscous forces prevail in the low- $Re$  flows. As mentioned above, turbulence defines most of the engineering flows with no exception for flows around vehicles and trucks. Thus, in vehicle aerodynamics, the  $Re$  is of the greatest importance for defining a flow field. In this case, the free-stream velocity and the characteristic dimension of the vehicle (width or height) are taken as  $\mathcal{U}$  and  $\mathcal{L}$  respectively.

Sections 3.1 and 3.2 present a summary of the main CFD approaches to simulating turbulent flows.

## 3.1 From DNS to RANS. Accuracy and efficiency

CFD uses different approaches to resolve a turbulent flow field. In general, the choice of the method is a compromise between the level of flow resolution and the computational resources available.

It is widely accepted that the equations system, known as Navier-Stokes Equations (NSE), mathematically determines the motion of fluids, although no mathematical proof exists for their universal validity. For an incompressible, single-phase flow with constant density  $\rho$  and viscosity  $\mu$ , the system reads:

$$\frac{\partial u_i}{\partial x_i} = 0 \quad (2)$$

$$\frac{\partial u_i}{\partial t} + u_j \frac{\partial u_i}{\partial x_j} = -\frac{1}{\rho} \frac{\partial p}{\partial x_i} + \nu \frac{\partial^2 u_i}{\partial x_j \partial x_j} + f_i. \quad (3)$$

Equation 2 is the continuity equation and expresses the mass conservation. Equation 3 are the momentum equations and express the momentum conservation.  $u_{i=x,y,z}$  are the three components of the velocity vector in a Cartesian coordinate system and  $p$  denotes the hydrodynamic pressure.  $\nu = \mu/\rho$  is the kinematic viscosity of the fluid and  $f_i$  are possible body forces (e.g. gravitational force). The NSE mathematically represent the large variety of flow structures (flow scales  $\kappa$ ) observed in a turbulent flow. Figure 11 shows the so called energy cascade process and how the flow scales are defined by their energy level  $E(\kappa)$ . Three main regions describe the aforementioned process. The energy is introduced in the flow by the largest eddies at the energy containing region (*I*) and consequentially transferred from larger to smaller eddies (typically anisotropic) through the entire inertial sub-range, (*II*). The energy is eventually dissipated into heat by the so called Kolmogorov scales (typically isotropic) in the dissipation range, (*III*).

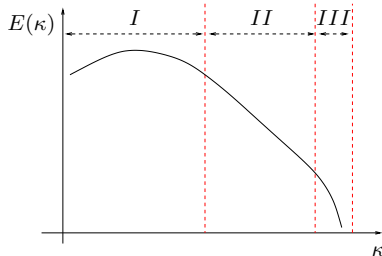


Figure 11: *The energy spectrum of a turbulent flow. Energy containing region (I), inertial subrange (II) and dissipative range (III)*

When the NSE are written in a discrete form and integrated numerically without modelling or hypothesis the direct numerical simulation (DNS) approach is used, [56]. DNS is the most accurate approach, but, it requires a prohibitive amount of computational resources to resolve all the scales present in a turbulent flow, from the largest to the Kolmogorov scales. As an example, a truck moving at cruise speed ( $Re = 3 \times 10^6$ ) produces a turbulent flow containing large structures of the dimension of  $10^0$ m and small structures of the dimension of  $10^{-9}$ m. Such a variety of scales make DNS infeasible for complex or high- $Re$  flows. Therefore, DNS is only used to study fundamental cases such as isotropic turbulence [57], turbulent boundary layer [58, 59] and pipe flow [60] to mention few. Nevertheless, different simplifications exist to enable solving Eqs. 2 and 3 in an affordable

manner. One of this is the so called Reynolds decomposition which splits up the flow in a mean and a fluctuating part as:

$$u_i = \bar{u}_i + u' \tag{4}$$

Inserting 4 into the NSE the Reynolds Averaged Navier-Stokes (RANS) equations are obtained

$$\frac{\partial \bar{u}_i}{\partial x_i} = 0 \tag{5}$$

$$\frac{\partial \bar{u}_i}{\partial t} + \bar{u}_j \frac{\partial \bar{u}_i}{\partial x_j} = -\frac{1}{\rho} \frac{\partial \bar{p}}{\partial x_i} + \frac{\partial}{\partial x_j} \left( \frac{\nu \partial \bar{u}_i}{\partial x_j} + \frac{1}{\rho} \tau_{ij} \right). \tag{6}$$

Here, an additional term, the so called Reynolds stress tensor, is obtained:

$$\tau_{ij} = -\rho \left( \overline{u'_i u'_j} \right). \tag{7}$$

The six new unknowns introduced by the tensor  $\tau_{ij}$  make the system impossible to solve in this form. Hence, the Reynolds stresses need to be modelled to close the problem. For this purpose the Boussinesq's assumption [61] is often used, to model the turbulent diffusion with a newly introduced eddy viscosity. This approach is widely used for applications of industrial importance. It resolves only the mean value of the flow, the large scales (region  $I$  in Fig. 11), modelling the entire cascade process and the dissipation. In this manner, the efficiency of the calculation increases to the detriment of the accuracy. Moreover, RANS provides a solution for the mean flow, and turbulence is treated in a stochastic sense only. Even though this is acceptable in many industrial applications, RANS cannot be used for a wide range of fields. Examples of such fields are active flow control [62], aeroacoustics [63], and fluid structures interaction studies [64].

If DNS and RANS are the antipodes of the simulation techniques, large eddy simulations (LES) and partially-averaged Navier-Stokes (PANS) represent good compromises between computer resources and accuracy. The central assumption of these methods is the scales' distinction in large and small scales. As mentioned above, the large scale motions carry most of the energy and the anisotropy of the flow, while the small scales represent the isotropic part of the turbulence and are responsible for the dissipation process. Hence, modelling the small scales and resolving the large ones benefits the overall result, reducing the simulation time as compared to DNS and improving the accuracy as compared to RANS.

## 3.2 Large eddy simulation and bridging methods

To achieve small/large scale separation, LES requires a filtering operation. As for the Reynolds decomposition, the LES filtering reformulates the expression of the instantaneous flow field,

$$u_i = \bar{u}_i + u'' \tag{8}$$

where the velocity field is decomposed in a resolved part  $\bar{u}_i$  and an unresolved or modelled part  $u''$ , also called sub grid scale (SGS). In LES, the mesh resolution defines the filtering, therefore, is of major importance to accurately design a fine enough grid that captures the

anisotropic features of the flow. (The LES model used throughout this thesis work is given in section 3.2.1). As follows, the grid point requirement for a good resolved LES scales with  $Re^{13/7}$ , as proposed by Choi and Moin [65], while Piomelli and Balaras [66] found the grid point estimation for a DNS scaling with  $Re^{9/4}$ . The LES estimation slightly relaxes the computational efforts as compared to DNS, yet it does not drastically decrease the cost. In fact, Spalart et al. [67] estimate that LES will be infeasible for an entire aircraft wing until the year 2045, and, they continue saying that *"terminating efforts in RANS turbulence modelling would be a very misguided step"*. For this reason, research in modelling must continue and the new frontier observed in recent years is hybrid models that thoughtfully blend DNS/LES and RANS approaches.

Bridging the gap between academic research and industrial R&D is of the greatest importance. The main challenge is to provide and develop a suitable and "intelligent" tool for industrial flow simulation, which independently switches its approach from DNS/LES to RANS, or better put, unsteady RANS (U-RANS), based on the available mesh resolution. The two main currents of bridging methods are the detached eddy simulation (DES) and the PANS approach, developed and modified in all their flavours during years. The first attempt to develop DES was introduced by Spalart et al. [67]. The basic idea is for the model to act as a U-RANS in boundary layers and LES-like otherwise. In principle, the LES or RANS choice is based on a comparison between the wall distance and the grid spacing. The main drawback of the behaviour as such is that DES grids need to be carefully designed, knowing a priori where the flow separates (LES should resolve the large separated vortices) and in which areas it remains attached (RANS boundary layer resolution). Many variations of this approach have been given during the years, and a review of variations and flavours is provided in [68]. Although zonal-like approaches have been shown great interest among many authors and developers with remarkable results [69–71], they are still limited concerning the adaptivity to the mesh. In other words, the mesh should always be designed carefully. The PANS approach was initially developed to overcome these difficulties and to make the solver acting like "independent" of the grid. The foundation of this method relies on the U-RANS approach. The goal of U-RANS is to resolve the fluctuations of the averaged flow, which are normally smoothed out by a steady RANS simulation. While the idea behind the method is promising, U-RANS gained an inaccurate prediction of severely separated flows. The main reason for this is that U-RANS lies on the evolution of the eddy viscosity, which evolves in large values, much larger than the actual mesh resolution could have supported. In this way, most of the temporal and spatial fluctuations are suppressed, altering the final solution. As an effort to resolve most of the fluctuating scales, the RANS coefficients must be modified according to the resolution of the grid, in a physically correct manner [72]. Modifying the parameters of the parent RANS model, PANS introduces a dynamic approach that prevents an uncontrolled growth (RANS-like result) or drop (resulting in spurious fluctuations) of the eddy viscosity, based on the spatial resolution of a given grid and the physics of the flow. The bright idea to develop a hybrid method as such started with the first PANS model based on the  $k - \varepsilon$  RANS equations [73]. The  $k - \varepsilon$  PANS method has been successfully tested on different standard bluff body flows, such as flow around a square cylinder [74] and a circular cylinder [75]. Theoretical proof and a physical explanation of his improvement in comparison with RANS is given in [72]. However, the quality of PANS depends also on

its RANS parent model. As a consequence, several flavours of the PANS method have been developed:

- Lakshminpathy and Girimaji [76] introduced the  $k - \omega$  PANS method. The results of this were compared with U-RANS showing that  $k - \omega$  PANS is able to resolve more vortical structures, enhancing the agreement with experimental data.
- Ma et al. [77] employed a low Reynolds number  $k - \varepsilon$  model to correct the standard  $k - \varepsilon$  PANS wall behaviour.
- Durbin [78] proposed a  $k - \varepsilon - \bar{v}^2 - f$  PANS, that was later reformulated by Hanjalic [79], to enhance the wall behaviour and take into account the Reynolds number effect in the viscous and buffer sub-layer.
- Basara et al. [80] proposed the  $k - \varepsilon - \zeta - f$  PANS developed on the namesake RANS model. The model has been validated for simple cases (channel flow), more complicated cases (flow around a finite cylinder and bluff bodies) [81–85] and even for real vehicle cases [86,87].

The latter flavour is also employed throughout this thesis work. Thus, a more detailed description is given in section 3.2.2.

### 3.2.1 The LES equations

The governing LES equations are the spatially implicitly filtered Navier-Stokes equations, where the spatial filter is determined by the characteristic width  $\Delta = (\Delta_1 \Delta_2 \Delta_3)^{\frac{1}{3}}$ , and  $\Delta_i$  is the computational cell size in the three coordinate directions.

$$\frac{\partial \bar{u}_i}{\partial x_i} = 0 \quad (9)$$

and

$$\frac{\partial \bar{u}_i}{\partial t} + \frac{\partial}{\partial x_j} (\bar{u}_i \bar{u}_j) = -\frac{1}{\rho} \frac{\partial \bar{p}}{\partial x_i} + \nu \frac{\partial^2 \bar{u}_i}{\partial x_j \partial x_j} - \frac{\partial \tau_{ij}}{\partial x_j}. \quad (10)$$

Here,  $\bar{u}_i$  and  $\bar{p}_i$  are the resolved velocity and pressure, respectively, and the bars over the variables denote the operation of filtering. The influence of the small scales in equation 10 appears in the SGS stress tensor,  $\tau_{ij} = \overline{u_i u_j} - \bar{u}_i \bar{u}_j$ . The algebraic eddy viscosity model, described in [88], was employed in this work. The Smagorinsky model represents the anisotropic part of the SGS stress tensor,  $\tau_{ij}$  as

$$\tau_{ij} - \frac{1}{3} \delta_{ij} \tau_{kk} = -2\nu_{sgs} \bar{S}_{ij} \quad (11)$$

where the SGS viscosity,

$$\nu_{sgs} = (C_s f_{vd} \Delta)^2 |\bar{S}| \quad (12)$$

and,

$$\bar{S} = \sqrt{(2\bar{S}_{ij} \bar{S}_{ij})} \quad (13)$$

where

$$\bar{S}_{ij} = \frac{1}{2} \left( \frac{\partial \bar{u}_i}{\partial x_j} + \frac{\partial \bar{u}_j}{\partial x_i} \right). \quad (14)$$

The Smagorinsky constant,  $C_s = 0.1$ , previously used in bluff body LES [89], is used in the present work.  $f_{vd}$ , in equation 12, is the Van Driest damping function,

$$f_{vd} = 1 - \exp\left(\frac{-n^+}{25}\right) \quad (15)$$

where  $n^+$  is the wall normal distance in viscous units.

### 3.2.2 PANS $k - \varepsilon - \zeta - f$

Before expressing the equations that define the model, it is necessary to recall Germano's averaging invariance property [90]. He stated that the SubFiltered Scale (SFS) term must be invariant to the type of filtering. Thus, if the filtering applied to the NSE is commutative with the spatio-temporal differential operator, and decomposing the turbulent velocity field  $V_i$ , by an arbitrary filter, in a resolved  $U_i$  and unresolved field  $u_i$ ,

$$V_i = U_i + u_i. \quad (16)$$

The NSE evolves according to [90] into the so called PANS equation [91]:

$$\frac{\partial U_i}{\partial t} + U_j \frac{\partial U_i}{\partial x_j} = -\frac{1}{\rho} \frac{\partial p}{\partial x_i} + \frac{\partial}{\partial x_j} \left( \nu \frac{\partial U_i}{\partial x_j} + \tau(V_i, V_j) \right), \quad (17)$$

where  $\tau(V_i, V_j)$  is the generalized second moment [90] and represents the effect of the unresolved scales on the resolved field. As for LES (see Eq. 11), the Boussinesq assumption is now invoked to model the second moment:

$$\tau(V_i, V_j) = -2\nu_u S_{ij} + \frac{2}{3} k_u \delta_{ij}. \quad (18)$$

Here,  $k_u$  is the unresolved kinetic energy,  $S_{ij}$  is the resolved stress tensor,

$$S_{ij} = \frac{1}{2} \left( \frac{\partial U_i}{\partial x_j} + \frac{\partial U_j}{\partial x_i} \right), \quad (19)$$

and  $\nu_u = C_\mu \zeta_u \frac{k_u^2}{\varepsilon_u}$  is the viscosity of the unresolved scales where  $\zeta_u = \overline{v_u^2}/k_u$  is the velocity scale ratio of the unresolved velocity scale  $\overline{v_u^2}$  and  $k_u$ .  $\overline{v_u^2}$  refers to the normal fluctuating component of the velocity field to any no-slip boundary. At this stage, three transport equations for  $k_u - \varepsilon_u - \zeta_u$  and a Poisson equation, for the elliptic relaxation function of the unresolved velocity scales, are necessary to close the model. The complete PANS

$k - \varepsilon - \zeta - f$  model is thus given by the following set of equations:

$$\begin{aligned}
\nu_u &= C_\mu \zeta_u \frac{k_u^2}{\varepsilon_u} \\
\frac{\partial k_u}{\partial t} + U_j \frac{\partial k_u}{\partial x_j} &= P_u - \varepsilon_u + \frac{\partial}{\partial x_j} \left( \frac{\nu_u}{\sigma_{k_u}} \frac{\partial k_u}{\partial x_j} \right) \\
\frac{\partial \varepsilon_u}{\partial t} + U_j \frac{\partial \varepsilon_u}{\partial x_j} &= C_{\varepsilon 1} P_u \frac{\varepsilon_u}{k_u} - C_{\varepsilon 2}^* \frac{\varepsilon_u^2}{k_u} + \frac{\partial}{\partial x_j} \left( \frac{\nu_u}{\sigma_{\varepsilon_u}} \frac{\partial \varepsilon_u}{\partial x_j} \right) \\
C_{\varepsilon 2}^* &= C_{\varepsilon 1} + f_k (C_{\varepsilon 2} - C_{\varepsilon 1}); \quad C_{\varepsilon 1} = 1.4 \left( 1 + \frac{0.045}{\sqrt{\zeta_u}} \right) \\
\frac{\partial \zeta_u}{\partial t} + U_j \frac{\partial \zeta_u}{\partial x_j} &= f_u - P_u \frac{\zeta_u}{k_u} + \frac{\zeta_u}{k_u} \varepsilon_u (1 - f_k) + \frac{\partial}{\partial x_j} \left( \frac{\nu_u}{\sigma_{\zeta_u}} \frac{\partial \zeta_u}{\partial x_j} \right) \\
L_u^2 \nabla^2 f_u - f_u &= \frac{1}{T_u} \left( c_1 + c_2 \frac{P_u}{\varepsilon_u} \right) \left( \zeta_u - \frac{2}{3} \right).
\end{aligned} \tag{20}$$

$P_u = -\tau(V_i, V_j) \frac{\partial U_i}{\partial x_j}$  is the production of the unresolved turbulent kinetic energy that is closed by the Boussinesq assumption, Eq. 18. The constants appearing in Eqs. 20 are:

$$C_\mu = 0.22; \quad C_{\varepsilon 2} = 1.9; \quad c_1 = 0.4; \quad c_2 = 0.65; \quad \sigma_k = 1; \quad \sigma_\varepsilon = 1.3; \quad \sigma_{\zeta_u} = 1.2.$$

$L_u$  and  $T_u$  are the length and time scales defined by using the unresolved kinetic energy:

$$T_u = \max \left[ \frac{k_u}{\varepsilon}, C_\tau \left( \frac{\nu}{\varepsilon} \right)^{1/2} \right]; \quad L_u = C_L \max \left[ \frac{k_u^{3/2}}{\varepsilon}, C_\eta \left( \frac{\nu^3}{\varepsilon} \right)^{1/4} \right],$$

where

$$C_\tau = 6; \quad C_L = 0.36; \quad C_\eta = 85.$$

A deeper explanation of the construction of the equations is given in [80, 81]. The parameters  $f_{k,\varepsilon}$  are the key factors that make the model act dynamically.  $f_{k,\varepsilon}$  are the ratios between resolved to total kinetic energy and dissipation, respectively, and they can assume values between 1 and 0 according to the selected cut-off. These parameters can be chosen a priori, knowing the resolution of the given grid. However, it might be more efficient to have a solver that adapts its accuracy to the flow case and the given grid, having as its worse output a RANS simulation. Here is indicated the importance of having a dynamic parameter that feels the characteristics of both the flow and the grid, adapting to the resolvable level of structures. For a further but justified simplification,  $f_\varepsilon$  is assumed to be constant and equal to 1. We recall the spatial resolution to resolve the dissipative scales, and the inertial sub-range is a near wall DNS resolution. These scales are unlikely to be resolved in most cases. Thus, all the unresolved dissipation is chosen to be RANS dissipation and is therefore modelled. Thus, the crucial step to developing an efficient model is the design of the last parameter  $f_k$ . Ideally, at every time-step for every computational cell, the simulation should measure the smallest value of  $f_k$  which the grid can support. Soon enough, the dynamic parameter was proposed as the ratio between

the geometric averaged grid cell dimension,  $\Delta = (\Delta_x \Delta_y \Delta_z)^{1/3}$ , and the Taylor scale of turbulence,  $\Lambda = \frac{(k_u + k_{res})^{3/2}}{\varepsilon}$  [92]:

$$f_k(x, t) = \frac{1}{\sqrt{C_\mu}} \left( \frac{\Delta}{\Lambda} \right)^{2/3}. \quad (21)$$

### 3.2.3 Numerical schemes

All types of numerical simulations require discretization of the spatial and temporal domain, and the choice of a suitable numerical scheme for every calculation is thus of main importance. In this work, the CFD simulations are carried out using the commercial finite volume software AVL-Fire. The NSE are discretized by the solver using a collocated grid arrangement. In the case of LES the convective term present in Eq. 10 is discretized using the central difference scheme (CDS) with a blending factor of 0.96, meaning that a 4% of a first order upwinding scheme is used to dampen the numerical oscillations and overcome the local insufficient grid resolution. In the case of PANS a second order upwinding scheme [93] is used for both the convective terms of the momentum equation and the turbulence closure system equations. The time discretization is done for all simulations using the implicit second order accurate three-time level scheme:

$$\left( \frac{d\phi}{dt} \right)_n = \frac{3\phi^n - 4\phi^{n-1} + \phi^{n-2}}{2\Delta t_n}; \quad \Delta t_n = t - t_{n-1} = t_{n-1} - t_{n-2}. \quad (22)$$

## 4 Experiments and wind tunnels

Besides the numerical work, three experimental campaigns were conducted in three different wind tunnel (WT) facilities. Experiments were performed on a concept scaled model at the Chalmers University WT. The facility is a close-loop WT with a test section of  $1.2 \times 1.8 \times 3 \text{ m}^3$  and a stable speed range of 0-60 m/s with an incoming flow turbulence level within 0.15%. Experiments were carried out at  $Re = 5 \times 10^5$ . The Canada research council WT is a full scale facility that allows measurement of the aerodynamic performance of a full scale truck (tractor and trailer) configuration. The test section measures  $9 \times 9 \times 24 \text{ m}^3$  and the inlet velocity varies within a range of 0-60 m/s. The experiments were carried out at real Reynolds number  $Re = 3.6 \times 10^6$ . The third, and ongoing, campaign is at the close-loop semi-industrial Valenciennes University WT, which is characterized by a  $2 \times 2 \times 10 \text{ m}^3$  test section and allows wind speeds in a range of 0-60 m/s. Similarly to the first campaign, the tests were carried out at  $Re = 5 \times 10^5$ .

Section 4.1 gives a summary of the measurement techniques used in this study.

### 4.1 Measurement techniques

Particle image velocimetry (PIV) images were recorded by a monochrome double-frame sCMOS camera SpeedSense M340 by Dantec with a  $2560 \text{ pixel} \times 1600 \text{ pixel}$  resolution, 12 bit pixel depth, and a  $10 \mu\text{m}$  pixel size. The camera was equipped with a 105mm f/2.8 lens from Sigma. The camera registered image pairs at a 400Hz frame rate at full resolution in double frame mode (with a time between pulses of  $60 \mu\text{s}$ ). The flow seeding was achieved with a fog generator and glycol based fluid. The Dual Power Nd:YLF LDY300-PIV laser from Litron provided up to  $2 \times 30 \text{ mJ}$  at 1000Hz and a 527nm wavelength. The laser was equipped with a laser guiding arm and laser sheet optics. The flow field area illuminated was  $200 \times 400 \text{ mm}^2$ . Dantec Dynamic Studio 2015 software was used for data acquisition and post-processing. Each data set included 800 images, which corresponded to a measurement period of two seconds with a spatial resolution of  $0.125 \times 0.156 \text{ mm}^2$  per pixel. The vector calculation was performed in multi-pass procedure with a decreasing window size. The initial interrogation window size was  $64 \text{ pixels} \times 64 \text{ pixels}$  with a 50% overlap and square 1:1 weighing factor for the first two passes. Finally, three passes were performed with a  $32 \text{ pixels} \times 32 \text{ pixels}$  window size, 50% overlap and round 1:1 Gaussian weighing factor. The velocity uncertainty was estimated as 0.1m/s for the time averaged velocity.

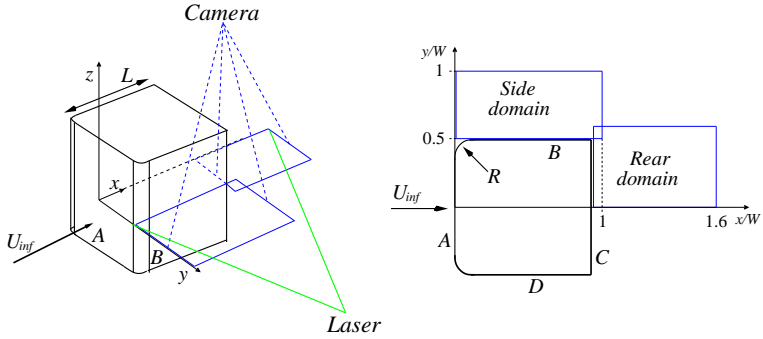


Figure 12: A sketch of the domains observed in experiments.

The experimental model was also equipped with horizontal and vertical arrays of pressure taps for the evaluation of the coefficient of pressure  $C_p$ . The pressure data were obtained using two 48-channel Scanivalve systems and the pressure system (NetScanner<sup>TM</sup> model 9116). The pressure system had an accuracy of  $\pm 0.2\text{Pa}$  for the pressure range studied ( $\pm 300\text{Pa}$ ). The pressure signals were time averaged over a period of 2s. Only the time averaged pressure values were used for the comparison with the CFD results. The aerodynamic force measurements of the full scale model were obtained with a six components external balance.

## 5 Modal decomposition

There are two main approaches to post-processing turbulence and turbulent flow data. One is the stochastic approach, which ignores the fluctuating part of the flow, Eq. 7, extracting only statistically relevant informations. The other is the phenomenological approach, which analyzes and interprets the interaction of coherent and incoherent flow structures highlighting possible universal or case specific turbulent patterns. In the framework of this project, the second approach is essential for two main reasons. The first motivation is that a statistical approach is insufficient for studying the effect of a time varying actuation (AFC) on a turbulent flow. The second reason is that, understanding the structure's interaction sets the guidelines for a thoughtful optimization process. The phenomenological approach gives hints and directions as to which are the main important structures acting in the flow, from both an energetic and a dynamic prospective. Modal and frequency decompositions are helpful tools for interpreting the flow mechanisms, that, for example, characterizes a pressure gradient induced separation. One of the patterns pursued in this work is therefore to employ proper orthogonal decomposition (POD) and fast Fourier transform (FFT) analysis to post-process CFD and experimental data.

The POD was developed independently for different disciplines (random variables, image processing, signal analysis chemical engineering and oceanography) by different authors. Among the first was Kosambi [94], but Lumley was the first to introduce POD in the context of turbulence [95]. An inspiring review of theory and applications of this method is presented in [96]. The POD used in this work, and increasingly commonplace in fluid dynamic research, is the POD snapshot methodology [97]. In the latter, an ensemble of snapshots from the selected flow field region was gathered and consequentially processed. The snapshot method was not only suitable for CFD data but was also largely employed in experiments, where the snapshots were collected by means of a high speed camera during a PIV [98,99]. Concerning CFD, several examples of successful POD applications can be found in the literature; modal decomposition has been applied to DNS data [100], LES [101,102] and hybrid methods (DES) [103].

The result of POD is not always straight-forward, and it is often complicated to recognize the dominant frequencies of every mode. Thus, in this work, POD is also coupled with FFT analysis on the same set of snapshots. FFT is a robust method, which once applied to snapshots, is able to spatially identify the main frequencies characterizing a flow. The result of this analysis confirms and completes the information extracted by POD. Thus, the POD and the FFT analysis are used to produce a spatial, energy and dynamic map of the main flow structures.

The present POD consists of equidistantly sampled 2D snapshots (pressure  $p$  or span-wise velocity component  $v$ )  $p^m = p(\mathbf{x}, t^m)$  at time  $t^m = m\Delta t$ ,  $m = 1, \dots, M$ , with the time  $\Delta t$ , and a Cartesian coordinate system  $\mathbf{x} = (x, y)$  with unit vectors  $\mathbf{e}_x$ ,  $\mathbf{e}_y$  respectively. As was originally proposed by Lumley [104], this method is based on an energy ranking of orthogonal structures computed from a correlation matrix of the snapshots. A singular value decomposition (SVD) approach is used to conduct the POD analysis on the given set of snapshots. In the present POD work, the variable (pressure  $p$  or span-wise velocity

component  $v$ ) is decomposed in the mean field,  $\langle p \rangle$ , and the fluctuating part,  $p'$ , as

$$p(\mathbf{x}, t) = \langle p \rangle(\mathbf{x}) + p'(\mathbf{x}, t). \quad (1)$$

The fluctuating part is then approximated, by the SVD approach, with space dependent modes,  $p_i$ , and a time dependent mode coefficient,  $b_i$ , as

$$p'(\mathbf{x}, t) = \sum_{i=1}^{\infty} b_i(t) p_i(\mathbf{x}) \approx \sum_{i=1}^{M-1} b_i(t) p_i(\mathbf{x}) + p_{res}(\mathbf{x}, t). \quad (2)$$

The definition can now be written in a more compact form if we consider that  $b_0 = 1$  and  $p_0 = \langle p \rangle$  following [105],

$$p(\mathbf{x}, t) = \sum_{i=0}^{M-1} b_i(t) p_i(\mathbf{x}). \quad (3)$$

The first and second moments of the POD modes coefficients are:

$$\langle b_i \rangle = 0; \quad \langle b_i b_j \rangle = \mu_i \delta_{ij}. \quad (4)$$

The energy content of the single mode,  $K_i$ , is approximated from the mode coefficients as

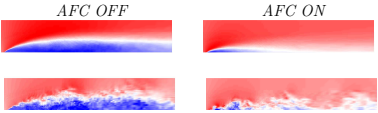
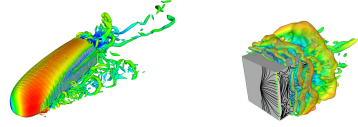
$$K_i(t) = \frac{1}{2} b_i^2(t), \quad (5)$$

and the total energy,  $K_{\Sigma}(t)$ , is evaluated as

$$K_{\Sigma}(t) = \sum_{i=1}^{M-1} K_i(t). \quad (6)$$

# 6 The work flow

Table 1: *The project timeline*

2014	<p><b>Phase 1:</b> preliminary LES on flow control</p> <ul style="list-style-type: none"> <li>- Separation mechanism</li> <li>- Controlled flow concept</li> </ul>	
2015	<p><b>Phase 2:</b> experiments on flow control</p> <ul style="list-style-type: none"> <li>- Design</li> <li>- WT measurements</li> </ul>	
2016	<p><b>Phase 3:</b> PANS validation</p> <ul style="list-style-type: none"> <li>- Test cases</li> <li>- Truck cabin case</li> </ul>	
	<p><b>Phase 4:</b> PANS for an oscillating cabin</p> <ul style="list-style-type: none"> <li>- Dynamic vs quasi-static</li> <li>- Actuated vs unactuated</li> </ul>	
2017	<p><b>Phase 5:</b> full scale test</p> <ul style="list-style-type: none"> <li>- AFC for a real truck</li> <li>- WT measurements</li> </ul>	
	<p><b>Phase 6:</b> micro-blower for AFC</p> <ul style="list-style-type: none"> <li>- Design</li> <li>- WT measurements</li> </ul>	
2017/12/08	<p>Ph.D. disputation</p>	

The work flow of the project can be divided into six intermediate goals achieved over the years. Table 1 shows the process timeline, and the next sections briefly explain the models and the achievements of each phase of the work.

## 6.1 Phase 1: preliminary LES on flow control

A preliminary LES study was conducted to investigate the truck A-pillar separation mechanism and its control. The computational domain consisted of a longitudinal section of a simplified truck model, Fig. 13

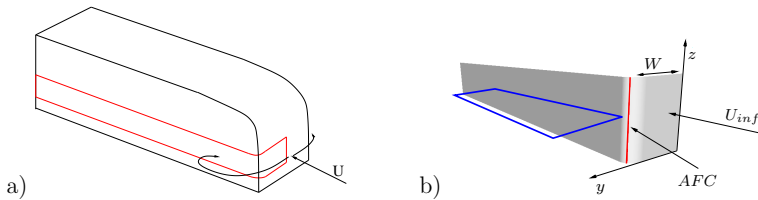


Figure 13: a) The longitudinal section of a simplified truck. b) The computational model. The blue rectangular area indicates the observed domain.

AFC is applied before the natural separation point of the flow. Results show the presence of an optimal actuation frequency that minimizes the separated region. For further details, see Paper A.

## 6.2 Phase 2: experiments on flow control

The experimental counterpart of phase 1 is necessary to study the applicability of this flow control. A simplified truck cabin is designed to contain four loud speakers that work as a flexible diaphragm in a sealed cavity. Figure 14 shows the assembly process of the model, while Fig. 15 shows the working principle of the actuation.

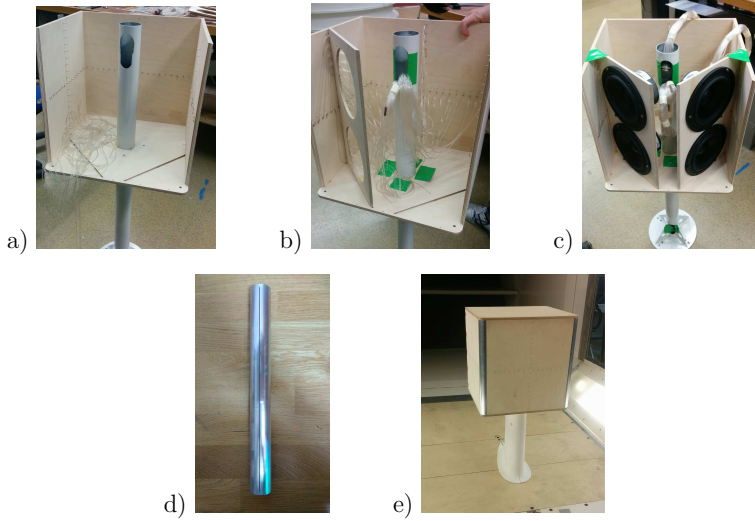


Figure 14: a) The side and the rear faces of the cabin are assembled. b) The pressure taps piping and the loud speaker's support. c) The loud speaker in place. d) The aluminium cylinder representing the A-pillar of the truck cabin. The cylinder has a 1mm slit to allow the actuation. e) The model is placed in the WT.

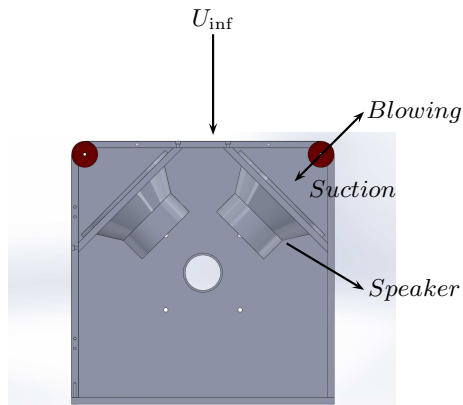


Figure 15: The working principle of the loud speaker flexible diaphragms.

As in phase 1, results show the presence of an optimal actuation frequency that minimizes the separated region. For further details, see Paper B.

### 6.3 Phase 3: PANS validation

PANS is validated in two test cases: a Willy's body case, Fig. 16a, and a surface mounted cube, Fig. 16b.

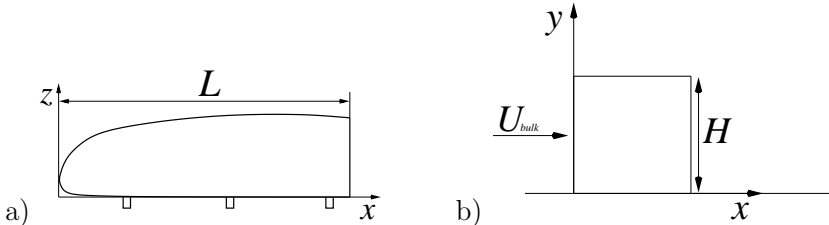


Figure 16: a) A side view of the Willy's body. b) A side view of the surface mounted cube model.

At a later stage, an extensive validation is carried out against in-house experiments (phase 2) and LES of the model presented in phase 2. Results show a good agreement of PANS with the experimental data and open the possibility to employ such a method for a more complicated flow case. For further details, see Papers C and D.

### 6.4 Phase 4: PANS for an oscillating cabin

PANS is used to study the effect of AFC on a dynamic oscillating configuration. The model is the same as used in phase 2. The oscillation of the model (Fig. 17) aims to reproduce a more realistic flow condition, where gusts created by overtaking, atmospheric turbulence and cross wind, significantly influence the incoming flow. A comparison between a quasi-static and the dynamic configuration is also proposed.

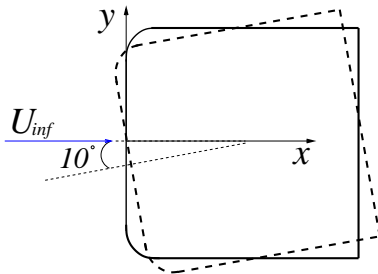


Figure 17: The rotation of the model during the simulation.

Overall, results show that the effect of the actuation is beneficial. The AFC decreases drag, stabilizes the flow and reduces the size of the side recirculation bubbles. For further details, see Paper E.

## 6.5 Phase 5: full scale test (unpublished results)

In this phase, AFC is applied to a real Volvo truck cabin, Fig. 18a. The interior of the cabin is equipped with a series of loudspeakers sealed in a cavity. Consequentially, a slot is open at the A-pillar, yellow dashed line in Fig. 18a. In this way, the same condition of the model used in phase 2 are recreated here. The complete full scale truck configuration (tractor plus trailer) is tested at the Canada research council WT, Fig. 18b. The aerodynamic performance and the flow are measured and analysed by means of force measurements and tufts visualizations, respectively. Starting from the aerodynamic forces, a drag decrease was observed along the whole yaw angle sweep, Fig. 19a. The truck was in fact tested at different yaw angles  $\beta$  and a maximum drag reduction of about 2% was observed at  $\beta = 0^\circ$  when the flow was actuated, Fig. 19b.

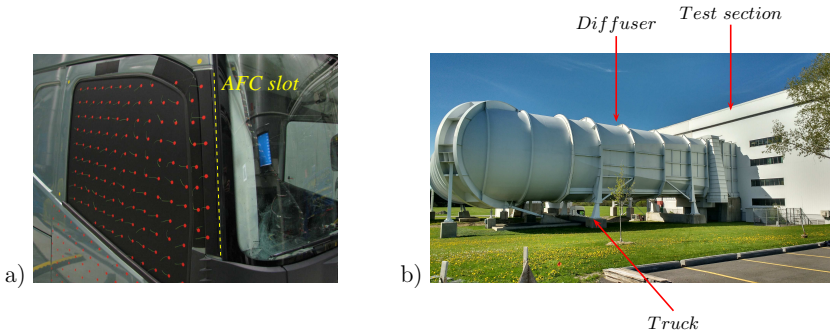


Figure 18: a) A particular of the truck cabin. The AFC slot is highlighted by a dashed yellow line. b) A particular of the the Canada research council WT. The truck is ready to be moved inside the test section.

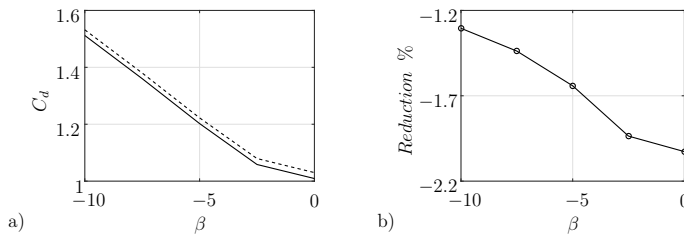


Figure 19: a)  $C_d$  comparison between actuated (solid line) and unactuated configuration (dashed line) at different yaw angles. b)  $C_d$  reduction (in %) at different yaw angles.

Flow visualizations on the side window of the truck was also performed at  $\beta = 0$ . Tufts were positioned on a black surface to improve the quality of the picture and facilitate the post processing of the data. Figure 20 shows a consecutive zoom of the area of interest that was investigated. Each tuft is attached with a red sticker, which is 15mm in diameter and approximately 0.3mm in thickness. The length of the tufts is about 35mm. The

tuft diameter used is approximately 1mm. Figure 21 shows post processed images of the observed area of two different cases: the pictures in the left column show the unactuated flow, while the pictures in the right column show the actuated flow case. A script was developed to post process the instantaneous pictures that captured tufts oscillations. Every set of pictures (500 snapshots) was first averaged for a traditional tufts analysis, Fig. 21(a-b). Higher perturbation regions show larger fluctuation of the interested tufts, resulting in a larger effective average tuft cone visualization. The averaged images are further post processed for a clearer flow visualization. The vector field represented by the direction of each tuft is superimposed in Fig. 21(c-d) and flow streak-lines are presented in Fig. 21(e-f). The analysis shows the benefit of the installed AFC. When the AFC is actuated, the flow is redirected along the stream-wise direction, and no reverse flow is visualised on the side of the truck. On the other hand, when the AFC is off, the flow is characterized by a strong vertical component and reverse flow.

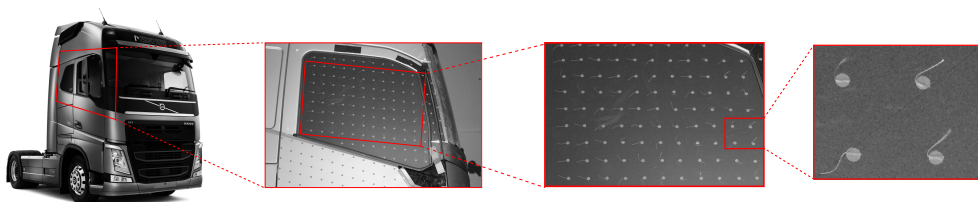


Figure 20: *A zoom of the observed domain. The tufts position is averaged and analysed over time.*

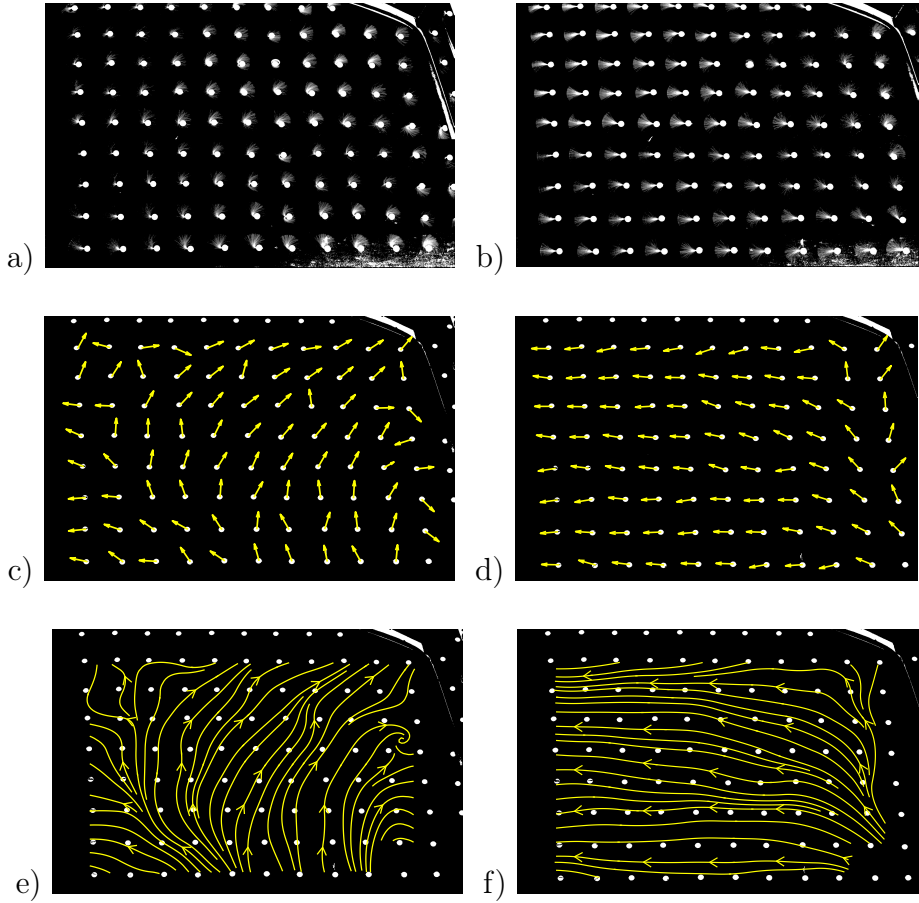


Figure 21: Average tufts tracking (a-b). Vector field visualization (c-d) and streak-lines (e-f); reconstruction from the average tuft tracking. AFC off (a, c and e). AFC on (b, d and f).

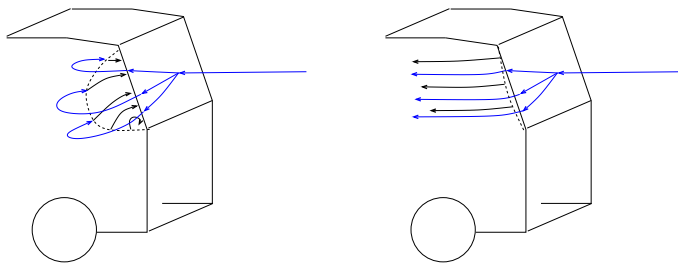


Figure 22: Interpretation of the flow topology under the effect of AFC. Left, AFC off. Right AFC on. Blue lines, external flow. Black solid lines, streamlines on the surface of the truck. The dashed black lines indicate the recirculation bubble region.

These last visualizations remain qualitative, yet they clearly show the strong effect of the AFC and they can be used to interpret the flow topology. Thus, an interpretation of the latter is attempted in Fig. 22. To conclude, an estimate of the net power gain is noteworthy. If  $P_0 = 200\text{kW}$  is the usual power consumption of a truck at cruise speed and the aerodynamic drag contributes for approximately 60% of the total power consumption, a drag reduction of 2% would in total save about 2.5kW. Now, considering that every of the six loudspeakers used 100W to function ( $P_{act} = 100 \times 6$ ), the net power-gain  $\Gamma$  can be estimated as follows:

$$\Gamma = \frac{P_0 \times 0.6 \times 0.02}{P_{act}} = \frac{2400}{600} = 4. \quad (1)$$

This figure shows a power gain larger than 1, therefore a net energy saving. Bearing in mind that the actuation was only applied along a short part of the cabin A-pillar (Fig. 18a), a future extension of this method, to other separated flow area of the truck surface, might bring to a larger energy saving and to a significant improvement of the aerodynamic performance of a heavy vehicle.

## 6.6 Phase 6: microblowers for AFC (unpublished results)

The latest, and ongoing, phase pursues the implementation of a smaller, silent and robust actuation. Commercial micro-blowers are used, Fig. 23. A complete characterization is provided in [106].



Figure 23: *The murata micro-blower device.*

The experiments were carried out in the Valenciennes University WT, using a modified version of the model used in phase 2. A new version of the aluminium cylinder used during phase 2 (Fig. 14d) was designed to host a series of microblowers along the A-pillar, Fig. 24 and 25. Figure 24 in particular, shows the CAD details of the new design while Fig. 25 shows the installed new device connected and functioning.



Figure 24: *Top, a section of the model from front and back views. The cylinder hosts the series of microblowers. Bottom, a zoom of the positioning of the microblowers.*

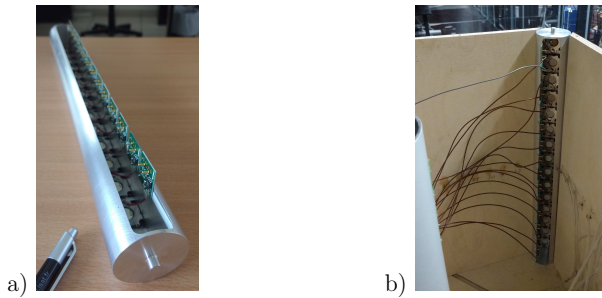


Figure 25: *a) The cylinder representative of the cabin A-pillar equipped with a series of microblowers. b) The cylinder placed in the cabin model.*

The diaphragm of this typology of actuators oscillates at a nominal frequency of 20kHz (this value lies out of the hearing human range). Hence, a second and lower frequency is superimposed to the nominal excitation frequency. The second frequency is directly applied to the supplied voltage of the actuators resulting in the signal represented in Fig. 26. Figure 26 gives only an indication of the output signal of the actuators, where  $T$  represents a period of the voltage modulation,  $U_{jet}$  is the variable jet velocity and  $U_{max}$  is the maximum output jet velocity.

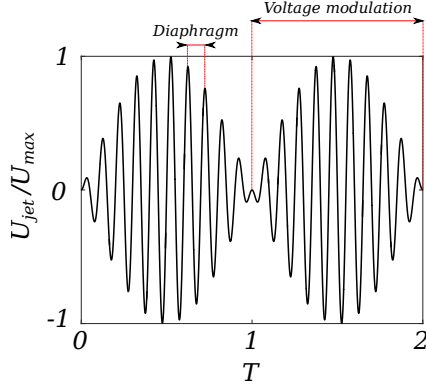


Figure 26: *En example of the microblower output signal.*

A preliminary experimental campaign involving PIV measurements is carried out at  $Re = 1.25 \times 10^5$ . The same side domain depicted in Fig. 12 was also observed in this experimental campaign. The microblowers affect strongly the recirculation bubble, Fig. 27. The actuation always affects the flow, reducing to different extents the thickness of the recirculation bubble. Moreover, the voltage modulation benefits the flow control. If no modulation is applied (Fig. 27,  $F^+ = 0$ ) the recirculation bubble is thicker when compared to all other modulated cases. Secondly, the highest reduction of the recirculation bubble thickness is obtained when the modulation frequency is  $F^+ = 4$ . This results describe a preliminary visualization of the microblower effect. The effectiveness of this kind of actuation at higher  $Re$  has to be tested and a deeper investigation of the flow physics is necessary to understand the optimal actuator's parameters. Nevertheless, the results introduced here are promising and represent a good starting point for a more detailed experimental campaign.

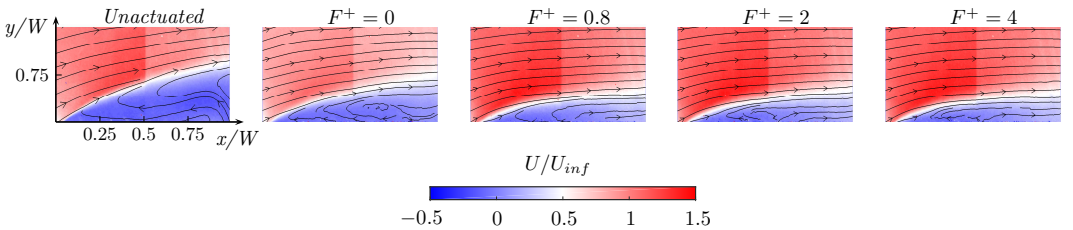


Figure 27: *Averaged streamwise velocity. The effect of the microblowers using different voltage modulations.*

## 7 Summary of Papers

The chapter gives summaries of the appended papers, outlining their aim and major results. Some additional comments are given along with the division of work between the authors.

### 7.1 Paper A

#### **Numerical Investigation of Active Flow Control Around a Generic Truck A-pillar**

**Aim:** To investigate the applicability of AFC to a pressure induced separated flow with a preliminary LES study

**Results:** A facing front-step geometry is used as a preliminary test case to verify the effectiveness of a synthetic jet to control the separation of the flow at the leading edge ( $Re = 1 \times 10^5$ ). The geometry is representative of a truck A-pillar. The position of the actuator was evaluated, as were different actuation frequencies. The AFC is most effective when it is positioned just before the separation point. Four actuation frequencies are tested and that show the importance of choosing the correct frequency. In particular, when the actuation is tuned to the shear layer separation frequency of the leading edge, the separation bubble is almost suppressed and the induced fluctuations by the actuation are minimized.

**Comments:** Part of this work was presented at:

- The 5th International Conference on Jets, Wakes and Separated Flows, ICJWSF2015, Stockholm, Sweden, 15-18 June 2015.
- The 8th International Symposium on Turbulence, Heat and Mass Transfer, September 15-18, 2015, Sarajevo, Bosnia and Herzegovina.

**Division of Work:** Guglielmo Minelli generated the computational mesh and set up, and ran and post-processed all simulations, wrote the POD scripts and wrote the paper. Co-authors provided priceless help with the writing of the paper and gave their support on all technical issues and data analysis.

### 7.2 Paper B

#### **Aerodynamic Flow Control for a Generic Truck Cabin Using Synthetic Jets**

**Aim:** To design a WT concept model representative of a truck cabin, and to control the A-pillar separation

**Results:** The flow around a truck cabin is characterized by pressure induced separation occurring at different areas. An experimental investigation conducted at  $Re = 5 \times 10^5$  was made to study the effect of an embedded AFC on the natural separation of the flow at the A-pillar of a simplified truck cabin model. Four actuation frequencies were studied and compared. The highest reduction of the recirculation was achieved when the actuation frequency was tuned to the shear layer separation frequency of the unforced flow. Moreover, the first three actuation frequencies have been seen to lock the side separation to the actuation frequency. Actuation frequencies out of the "receptive band" of unforced frequencies of the flow do not show a lock-in behaviour, but a higher value of the momentum coefficient is required to control the separation to the same extent.

**Comments:** Part of the work was presented at:

- The European Drag Reduction and Flow Control Meeting – EDRFCM 2017 April 3–6, 2017, Rome, Italy.

**Division of Work:** Guglielmo Minelli and Erwin Hartono designed, set up and ran the WT experiments. Volvo trucks manufactured the model. Guglielmo Minelli post-processed the WT data and wrote the paper. All co-authors provided priceless help with the writing of the paper and gave their support in all technical issues and data analysis.

## 7.3 Paper C

### Partially-averaged Navier–Stokes Simulations of Two Bluff Body Flows

**Aim:** To validate the PANS numerical method on test cases for further simulations

**Results:** Two test cases were used to study and validate the PANS predictions of heavily separated flows. A surface mounted cube (SFC) and a Willy's body were employed. There is a sufficient amount of experimental data and previous numerical data (published by different authors) that can be used for the validation of these two geometries. Thus, LES, PANS, URANS and experimental data are compared in terms of predicted flow structures. A grid refinement study conducted on both geometries shows the adaptability of the PANS method to the grid employed. A larger portion of the turbulence is modelled with a coarser mesh, while, refining the mesh, more and more turbulent structures are resolved. Considering the SFC case, a comparison between LES, PANS and URANS in terms of predicted turbulent flow structures and predicted flow scales is also reported. It is shown how PANS can adapt to the grid refinement and how resolved viscosity, production and Taylor scale change according to the method and the grid refinement.

**Comments:** Part of the work was presented at:

- ICNAAM 2014, The 12th International Conference of Numerical Analysis and Applied Mathematics, Rhodes, Greece, Sep 22-28, 2014.

**Division of Work:** Guglielmo Minelli generated the computational meshes, set up, ran and post-processed all simulations. Siniša Krajnović wrote the paper. All co-authors provided priceless help with their support in all technical issues and data analysis.

## 7.4 Paper D

### Validation of PANS and Active Flow Control for a Generic Truck Cabin

**Aim:** To validate the PANS numerical method in a specific WT model representative of a truck cabin

**Results:** PANS simulations, at  $Re = 5 \times 10^5$ , were conducted to analyze an active flow control strategy for a generic truck cabin. The PANS approach was validated against experiments and resolved LES, showing the potential of capturing the main flow features, when a mesh, far from being resolved for LES, was employed. Overall, the validation demonstrates a better prediction by PANS when a drastically coarsen grid is used, and a good prediction of the main important structures and frequencies of the flow field was obtained. After this process, the main frequencies and POD modes are individuated for the unactuated case. Thus, the frequencies describing the first three most energetic pressure POD modes were used to actuate the flow. When the actuation frequency described the shear layer instability, the highest drag reduction, a suppression of the separation bubble, and the lowest induced artificial fluctuations are observed. In addition, the structures generated by different actuation frequencies are found to be substantially different. A low actuation frequency forms structures that have a uniform elongated vortex core along the A-pillar. In contrast, the disturbances of higher actuation frequencies form smaller and less organized hairpin like vortical structures.

**Comments:** Part of the work was presented at:

- The 16th European Turbulence Conference, 21-24 August, 2016, Stockholm, Sweden.

**Division of Work:** Guglielmo Minelli and Erwin Hartono designed, set up and ran the WT experiments. Volvo trucks manufactured the model. Guglielmo Minelli generated the computational meshes, set up and ran the simulations, wrote the POD scripts, post-processed the WT and numerical data and wrote the paper. All co-authors provided priceless help with the writing of the paper and gave their support on all technical issues and data analysis.

## 7.5 Paper E

### A Flow Control Study of a Simplified, Oscillating Truck Cabin using PANS

**Aim:** To verify the effectiveness of AFC under severe flow conditions using PANS.

**Results:** This work presents an application of the partially-averaged Navier-Stokes (PANS) equations for an external vehicle flow. In particular, the flow around a generic truck cabin is simulated. The PANS method is first validated against experiments and resolved LES of two static cases. As a consequence, PANS is used to study the effect of an active flow control (AFC) on a dynamic oscillating configuration. The oscillation of the model represents a more realistic ground vehicle flow, where gusts (of different natures) define the unsteadiness of the incoming flow. In the numerical study, the model is forced to oscillate with a yaw angle  $-10^\circ < \beta < 10^\circ$  and a non-dimensional frequency  $St = fW/U_{inf} = 0.1$ . The effect of the periodic motion of the model is compared with the quasi-static flow condition. At a later stage, the dynamic configuration is actuated by means of a synthetic jet boundary condition. Overall, the effect of the actuation is beneficial. The actuation of the AFC decreases drag, stabilizes the flow and reduces the size of the side recirculation bubbles.

**Comments:** Part of the work was presented at:

- Proceedings of the ASME 2017 Fluids Engineering Division Summer Meeting FEDSM2017 July 30-August 3, 2017, Waikoloa, USA.

**Division of Work:** Guglielmo Minelli generated the computational meshes, set up and ran the simulations, post-processed the numerical data and wrote the paper. All co-authors provided priceless help with the writing of the paper and gave their support on all technical issues and data analysis.

## 7.6 Paper F

### Development of Active Flow Control for Trucks

**Aim:** To summarize and describe the work flow of the development of an active flow control strategy for a real truck.

**Results:** The development of this technique and its effectiveness were tackled in a multi-disciplinary way. The AFC achievements observed in numerical simulations were corroborated by experimental data, and the conceptual flow structure mechanism found its counterpart in the analysis of the aerodynamic performance of a real vehicle. First, LES demonstrated the efficacy of the AFC in a very simplified case. Second, a consistent study of PANS was conducted. PANS was validated and subsequently used for dynamic simulations. Third, the flow control was implemented and tested on a real Volvo truck cabin. In conclusion, the stages covered in the paper show promising AFC results in terms of drag reduction and also show the possibility for an extensive applicability of AFC to road vehicles.

**Comments:** The work was presented at:

- 3rd Thermal and Fluids Engineering Conference (TFEC), March 4–7, 2018, Fort Lauderdale, FL, USA.

**Division of Work:** Guglielmo Minelli generated the computational meshes, set up and ran the simulations, post-processed the numerical data and wrote the paper. Guglielmo Minelli and Erwin Hartono designed, set up and ran the WT experiments. Volvo trucks manufactured the model and performed the full scale experiments. All co-authors provided priceless help with the writing of the paper and gave their support on all technical issues and data analysis.



## 8 Conclusion and Future Directions

Here it has been described the importance and the potential of an AFC when applied to road vehicles. The development of this technique and its effectiveness were tackled in a multi-disciplinary way. The AFC achievements observed in numerical simulations were corroborated by experimental data, and the conceptual flow structure mechanism found its counterpart in the analysis of the aerodynamic performance of a real vehicle. The project time line can be divided into three macro stages.

First, LES demonstrated the efficacy of the AFC in a very simplified case. Even though the model used for the simulations was removed from geometrical complexities, the study gave important directions for the design of the experimental demonstrator model (representative of a truck cabin) equipped with AFC. The AFC ability to improve the aerodynamic performance of the model was remarkable. Moreover, the interaction between the actuation and the surrounding flow is crucial for a successful implementation. The AFC actuation frequency and magnitude are in fact the main players in the game and they need to be tuned toward an optimal flow control.

Second, a consistent study of PANS was conducted. PANS is a promising numerical tool that blends the accuracy of an LES with the efficiency of RANS. As such, the method was tested and validated on three different models: a surface mounted cube, a Willy's body and a truck cabin model used in the previous WT experiments. In all these cases, the results show good agreement with experimental data. Therefore, PANS was used to simulate a controlled flow under the effect of gusts. The AFC was demonstrated to improve the aerodynamic performance under discussed flow conditions as well.

Third, the flow control was implemented and tested on a real Volvo truck cabin. At this stage, the same AFC principle used for the demonstrator was applied here. Tufts flow visualizations and aerodynamic force measurements of a full scale test confirm the beneficial effect of the AFC, resulting in a net gain between the power spent for the actuation and the power saved by drag reduction.

In conclusion, the stages covered so far show promising AFC results in terms of drag reduction and also show the possibility for an extensive applicability of AFC for road vehicles. Nevertheless, smaller and more efficient devices need to be investigated for a real implementation. An investigation of micro-blowers is ongoing and, once their robustness is tested, they would be a good candidate for a broader implementation.

# References

- [1] “A European Strategy for Low-Emission Mobility,” *COM(2016) 501*, 2016.
- [2] J. D. Anderson, *Introduction to Flight*. 2005.
- [3] R. M. Wood, “A Discussion of a Heavy Truck Advanced Aerodynamic Trailer System,” in *International Forum for Road Transport Technology (IFRTT) 9th International Symposium on Heavy Vehicle Weights and Dimensions.*, 2006.
- [4] D. Söderblom, L. Löfdahl, P. Elofsson, and L. Hjelm, “Heavy Vehicle Wheel Housing Flows - a Parametric Study,” *SAE Technical Paper*, 2009.
- [5] D. Söderblom, P. Elofsson, L. Hjelm, and L. Löfdahl, “Wheel Housing Aerodynamics on Heavy Trucks BT - The Aerodynamics of Heavy Vehicles III: Trucks, Buses and Trains,” pp. 211–223, Cham: Springer International Publishing, 2016.
- [6] M. Gad-el Hak, “Introduction to flow control,” *Flow Control*, no. 1904, pp. 1–107, 1998.
- [7] L. Prandtl, “ber Flüssigkeitsbewegung bei sehr kleiner Reibung,” *Verhandlungen des dritten internationalen MathematikerKongresses*, vol. Heidelberg, pp. 484–491, 1904.
- [8] K. Cooper, “The effect of front-edge rounding and rear-edge shaping on the aerodynamic drag of bluff vehicles in ground proximity,” 1985.
- [9] K. Cooper, “Truck Aerodynamics Reborn - Lessons from the Past,” *SAE Technical Paper Series*, 2003.
- [10] M. El-alti, V. Chernoray, M. Jahanmiri, and L. Davidson, “Experimental and Computational Studies of Active Flow Control on a Model Truck-trailer,” *EPJ Web of Conferences 25*, vol. 010, 2012.
- [11] J. Kehs, K. Visser, J. Grossmann, C. Horrell, and A. Smith, “Experimental and Full Scale Investigation of Base Cavity Drag Reduction Devices for Use on Ground Transport Vehicles BT - The Aerodynamics of Heavy Vehicles III: Trucks, Buses and Trains,” pp. 269–283, Cham: Springer International Publishing, 2016.
- [12] R. Pankajakshan, C. B. Hilbert, and D. L. Whitfield, “Passive Devices for Reducing Base Pressure Drag in Class 8 Trucks BT - The Aerodynamics of Heavy Vehicles III: Trucks, Buses and Trains,” pp. 227–235, Cham: Springer International Publishing, 2016.
- [13] R. Wood and S. Bauer, “Simple and low-cost aerodynamic drag reduction devices for tractor-trailer trucks,” *SAE transactions*, vol. 112, no. 2, pp. 143–160, 2003.
- [14] B. Khalighi, S. Zhang, C. Koromilas, S. R. Balkanyi, L. P. Bernal, G. Iaccarino, and P. Moin, “Experimental and Computational Study of Unsteady Wake Flow Behind a Bluff Body with a Drag Reduction Device,” *Society of automotive engineers*, no. 724, pp. 1–15, 2001.
- [15] R. Verzicco, M. Fatica, G. Iaccarino, P. Moin, and B. Khalighi, “Large Eddy Simulation of a Road Vehicle with Drag-Reduction Devices,” *AIAA Journal*, vol. 40, no. 12, pp. 2447–2455, 2002.

- [16] G. M. R. van Raemdonck and M. J. L. van Tooren, “Numerical and Wind Tunnel Analysis Together with Road Test of Aerodynamic Add-Ons for Trailers BT - The Aerodynamics of Heavy Vehicles III: Trucks, Buses and Trains,” pp. 237–252, Cham: Springer International Publishing, 2016.
- [17] J. D. Coon and K. D. Visser, “Drag Reduction of a Tractor-Trailer Using Planar,” *The Aerodynamic of Heavy Vehicles: Trucks, Buses, and Trains*, vol. 1, 2004.
- [18] S. Krajnović, “Large Eddy Simulation Exploration of Passive Flow Control Around an Ahmed Body,” *ASME Journal of Fluids Engineering*, vol. 136, p. 121103, sep 2014.
- [19] L. N. Cattafesta and M. Sheplak, “Actuators for Active Flow Control,” *Annual Review of Fluid Mechanics*, vol. 43, pp. 247–272, 2011.
- [20] S. L. Brunton and B. R. Noack, “Closed-Loop Turbulence Control: Progress and Challenges,” *Applied Mechanics Reviews*, vol. 67, 2015.
- [21] R. Simpson, “Turbulent Boundary-Layer Separation,” *Annual Review of Fluid Mechanics*, vol. 21, no. 1, pp. 205–234, 1989.
- [22] R. L. Simpson, “Aspects of turbulent boundary-layer separation,” *Progress in Aerospace Sciences*, vol. 32, no. 5, pp. 457–521, 1996.
- [23] V. J. Modi and V. S. Deshpande, “Fluid dynamics of a cubic structure as affected by momentum injection and height,” *Journal of Wind Engineering and Industrial Aerodynamics*, vol. 89, no. 5, pp. 445–470, 2001.
- [24] S. Mittal, “Flow Control Using Rotating Cylinders: Effect of Gap,” *Journal of Applied Mechanics*, vol. 70, no. 5, p. 762, 2003.
- [25] X. Han and S. Krajnović, “Large Eddy Simulation of Flow Control Around a Cube Subjected to Momentum Injection,” *Flow, Turbulence and Combustion*, vol. 92, pp. 527–542, apr 2013.
- [26] J. C. Schulmeister, J. M. Dahl, G. D. Weymouth, and M. S. Triantafyllou, “Flow control with rotating cylinders,” *Journal of Fluid Mechanics*, vol. 825, pp. 743–763, aug 2017.
- [27] S. Krajnović, J. Östh, and B. Basara, “LES study of breakdown control of A-pillar vortex,” *International Journal of Flow Control*, vol. 2, pp. 237–258, 2010.
- [28] D. Barros, J. Borée, B. R. Noack, A. Spohn, and T. Ruiz, “Bluff body drag manipulation using pulsed jets and Coanda effect,” *Journal of Fluid Mechanics*, vol. 805, pp. 422–459, 2016.
- [29] G. Lubinsky and A. Seifert, “Suction and Oscillatory Blowing Applied to the Rounded Front Edges of a Square Prism BT - Instability and Control of Massively Separated Flows: Proceedings of the International Conference on Instability and Control of Massively Separated Flows, held in P,” pp. 157–162, Cham: Springer International Publishing, 2015.
- [30] A. Seifert, I. Dayan, C. Horrell, J. Grossmann, and A. Smith, “Heavy Trucks Fuel Savings Using the SaOB Actuator BT - The Aerodynamics of Heavy Vehicles III: Trucks, Buses and Trains,” pp. 377–390, Cham: Springer International Publishing, 2016.

- [31] B. L. Smith and A. Glezer, “The formation and evolution of synthetic jets,” *Physics of Fluids (1994-present)*, vol. 10, no. 9, pp. 2281–2297, 1998.
- [32] J. R. Roth, D. M. Sherman, and S. P. Wilkinson, “Boundary layer flow control with a one atmosphere uniform glow discharge surface plasma,” *36th Aerospace Sciences Meeting & Exhibit January*, vol. 28, 1998.
- [33] E. Moreau, “Airflow control by non-thermal plasma actuators,” *Journal of Physics D: Applied Physics*, vol. 40, no. 3, pp. 605–636, 2007.
- [34] T. C. Corke, C. L. Enloe, and S. P. Wilkinson, “Dielectric Barrier Discharge Plasma Actuators for Flow Control,” *Annual Review of Fluid Mechanics*, vol. 42, no. 1, pp. 505–529, 2010.
- [35] N. Benard and E. Moreau, “Electrical and mechanical characteristics of surface AC dielectric barrier discharge plasma actuators applied to airflow control,” *Experiments in Fluids*, vol. 55, no. 11, 2014.
- [36] J. A. Vernet, *Plasma actuators for separation control on bluff bodies*. PhD thesis, Mechanics, School of Engineering Sciences (SCI), KTH, 2017.
- [37] R. E. Hanson, P. Lavoie, A. M. Naguib, and J. F. Morrison, “Transient growth instability cancelation by a plasma actuator array,” *Experiments in Fluids*, vol. 49, no. 6, pp. 1339–1348, 2010.
- [38] M. Amitay and A. Glezer, “Role of Actuation Frequency in Controlled Flow Reattachment over a Stalled Airfoil,” *AIAA Journal*, vol. 40, pp. 209–216, 2002.
- [39] D. R. Smith, “Interaction of a Synthetic Jet with a Cross ow Boundary Layer,” *AIAA Journal*, vol. 40, pp. 2277–2288, 2002.
- [40] D. You and P. Moin, “Active control of flow separation over an airfoil using synthetic jets,” *Journal of Fluids and Structures*, vol. 24, pp. 1349–1357, nov 2008.
- [41] A. Glezer, “Some aspects of aerodynamic flow control using synthetic-jet actuation.,” *Philosophical transactions. Series A, Mathematical, physical, and engineering sciences*, vol. 369, pp. 1476–94, 2011.
- [42] A. Brumm and W. Nitsche, “Active control of turbulent separated flows over slanted surfaces,” *International Journal of Heat and Fluid Flow*, vol. 27, pp. 748–755, 2006.
- [43] M. Ben Chiekh, M. Ferchichi, M. Michard, M. S. Guellouz, and J. C. Béra, “Synthetic jet actuation strategies for momentumless trailing edge wake,” *Journal of Wind Engineering and Industrial Aerodynamics*, vol. 113, pp. 59–70, 2013.
- [44] S. Krajnović and J. Fernandes, “Numerical simulation of the flow around a simplified vehicle model with active flow control,” *International Journal of Heat and Fluid Flow*, vol. 32, pp. 192–200, feb 2011.
- [45] S. Watkins and J. W. Saunders, “Turbulence Experienced by Road Vehicles under Normal Driving Conditions,” *SAE Technical Paper Series*, 1995.
- [46] S. Wordley and J. Saunders, “On-road Turbulence,” 2008.
- [47] S. Wordley and J. Saunders, “On-road Turbulence: Part 2,” vol. 2, no. 1, pp. 111–137, 2009.

- [48] L. W. Sigurdson and A. Roshko, “The Structure and Control of a Turbulent Reattaching Flow,” *Turbulence Management and Relaminarisation*, pp. 497–514, 1988.
- [49] K. Sasaki and M. Kiya, “Three-Dimensional Vortex Structure in a Leading-Edge Separation Bubble at Moderate Reynolds Numbers,” *ASME Journal of Fluids Engineering*, vol. 113, pp. 405–410, sep 1991.
- [50] A. Siefert, T. Bachar, D. Koss, M. Shepshelovich, and I. Wygnanski, “Oscillatory blowing: A tool to delay boundary-layer separation,” *AIAA journal*, vol. 31, no. 11, pp. 2052–2060, 1993.
- [51] J.-Z. Wu, X.-Y. Lu, A. G. Denny, M. Fan, and J.-M. Wu, “Post-stall flow control on an airfoil by local unsteady forcing,” *Journal of Fluid Mechanics*, vol. 371, pp. 21–58, 1998.
- [52] A. Glezer, M. Amitay, and A. M. Honohan, “Aspects of Low- and High-Frequency Actuation for Aerodynamic Flow Control,” *AIAA Journal*, vol. 43, pp. 1501–1511, 2005.
- [53] M. F. Unal and D. Rockwell, “On vortex formation from a cylinder. Part 1. The initial instability,” *Journal of Fluid Mechanics*, vol. 190, pp. 491–512, 1988.
- [54] S. B. Pope, *Turbulent Flows*. 2001.
- [55] O. Reynolds, “On the dynamical theory of incompressible viscous fluids and the determination of the criterion,” *Philos. Trans. R. Soc. London*, vol. 186, pp. 123–164.
- [56] S. Kurien and M. a. Taylor, “Direct Numerical Simulations of Turbulence Data Generation and Statistical Analysis,” *Los A*, no. 29, pp. 142–151, 2005.
- [57] T. Ishihara, T. Gotoh, and Y. Kaneda, “Study of high-Reynolds number isotropic turbulence by direct numerical simulation,” *Annual Review of Fluid Mechanics*, vol. 41, no. 1, pp. 165–180, 2009.
- [58] T. Ishihara, Y. Kaneda, M. Yokokawa, K. Itakura, and A. Uno, “Small-scale statistics in high-resolution direct numerical simulation of turbulence: Reynolds number dependence of one-point velocity gradient statistics,” *Journal of Fluid Mechanics*, vol. 592, pp. 335–366, 2007.
- [59] P. Schlatter and R. Örlü, “Assessment of direct numerical simulation data of turbulent boundary layers,” *Journal of Fluid Mechanics*, vol. 659, pp. 116–126, 2010.
- [60] J. Ahn, J. H. Lee, J.-h. Kang, and H. J. Sung, “Direct numerical simulation of a 30R long turbulent pipe flow at  $R^+ = 685$ : large- and very large-scale motions,” *Physics of Fluids*, vol. 27, p. 065110, 2015.
- [61] J. Boussinesq, “Essai sur la théorie des eaux courantes,” *Imprimerie nationale*, vol. 2, 1877.
- [62] M. El-Alti, *Active Flow Control for Drag Reduction of Heavy Vehicles*. Department of Applied Mechanics, Fluid Dynamics, Chalmers University of Technology, 2012.
- [63] H. Hafsteinnsson, *Study of Supersonic Jet Noise Reduction using LES*. Department of Applied Mechanics, Fluid Dynamics, Chalmers University of Technology, 2014.

- [64] J. Östh, *Unsteady Numerical Simulations and Reduced-Order Modelling of Flows around Vehicles*. Department of Applied Mechanics, Fluid Dynamics, Chalmers University of Technology, 2014.
- [65] H. Choi and P. Moin, “Grid-point requirements for large eddy simulation: Chapman’s estimates revisited,” *Physics of Fluids*, vol. 24, no. 1, pp. 13–18, 2012.
- [66] U. Piomelli and E. Balaras, “Wall-Layer Models for Large Eddy Simulations,” *Annual Review of Fluid Mechanics*, vol. 34, pp. 349–374, 2002.
- [67] P. R. Spalart, W. H. Jou, M. Strelets, and S. R. Allmaras, “Comments on the feasibility of LES for wings and on a hybrid RANS/LES approach,” in *Advances in DNS/LES*, vol. 1, pp. 4–8, 1997.
- [68] B. Nebenführ, *Turbulence-resolving simulations for engineering applications*. Department of Applied Mechanics, Fluid Dynamics, Chalmers University of Technology, 2015.
- [69] L. Davidson and S. H. Peng, “Hybrid LES-RANS modelling: A one-equation SGS model combined with a k-w model for predicting recirculating flows,” *International Journal for Numerical Methods in Fluids*, vol. 43, no. 9, pp. 1003–1018, 2003.
- [70] S. H. Peng, “Hybrid RANS-LES modeling based on zero- and one-equation models for turbulent flow simulation,” in *4th International Symposium on Turbulence and Shear Flow Phenomena*, vol. 3, pp. 1159–1164, 2005.
- [71] P. R. Spalart, S. Deck, M. L. Shur, K. D. Squires, M. K. Strelets, and A. Travin, “A new version of detached-eddy simulation, resistant to ambiguous grid densities,” *Theoretical and Computational Fluid Dynamics*, vol. 20, no. 3, pp. 181–195, 2006.
- [72] S. S. Girimaji, E. Jeong, and R. Srinivasan, “Partially Averaged Navier-Stokes Method for Turbulence: Fixed Point Analysis and Comparison With Unsteady Partially Averaged Navier-Stokes,” *Journal of Applied Mechanics*, vol. 73, no. 3, p. 422, 2006.
- [73] S. S. Girimaji, “Partially-Averaged Navier-Stokes Model for Turbulence: A Reynolds-Averaged Navier-Stokes to Direct Numerical Simulation Bridging Method,” *Journal of Applied Mechanics*, vol. 73, no. 3, p. 413, 2006.
- [74] E. Jeong and S. S. Girimaji, “Partially Averaged Navier–Stokes (PANS) Method for Turbulence Simulations—Flow Past a Square Cylinder,” *ASME Journal of Fluids Engineering*, vol. 132, no. 12, p. 121203, 2010.
- [75] S. Lakshmipathy and S. S. Girimaji, “Partially Averaged Navier–Stokes (PANS) Method for Turbulence Simulations: Flow Past a Circular Cylinder,” *ASME Journal of Fluids Engineering*, vol. 132, no. 12, p. 121202, 2010.
- [76] S. Lakshmipathy and S. Girimaji, “Partially-averaged Navier-Stokes method for turbulent flows: k-w model implementation,” in *44th AIAA Aerospace Sciences Meeting and Exhibit*, Aerospace Sciences Meetings, American Institute of Aeronautics and Astronautics, jan 2006.
- [77] J. M. Ma, S. H. Peng, L. Davidson, and F. J. Wang, “A low Reynolds number variant of partially-averaged Navier-Stokes model for turbulence,” *International Journal of Heat and Fluid Flow*, vol. 32, no. 3, pp. 652–669, 2011.

- [78] P. A. Durbin, "Near-wall turbulence closure modeling without "damping functions"," *Theoretical and Computational Fluid Dynamics*, vol. 3, no. 1, pp. 1–13, 1991.
- [79] K. Hanjalić, M. Popovac, and M. Hadžiabdić, "A robust near-wall elliptic-relaxation eddy-viscosity turbulence model for CFD," *International Journal of Heat and Fluid Flow*, vol. 25, pp. 1047–1051, dec 2004.
- [80] B. Basara, S. Krajnović, and S. Girimaji, "PANS methodology applied to elliptic-relaxation based eddy viscosity transport model," *Turbulence and Interactions*, pp. 63–69, 2010.
- [81] B. Basara, S. Krajnovic, S. Girimaji, and Z. Pavlovic, "Near-Wall Formulation of the Partially Averaged Navier Stokes Turbulence Model," *AIAA Journal*, vol. 49, pp. 2627–2636, 2011.
- [82] S. Krajnović, R. Lárusson, and B. Basara, "Superiority of PANS compared to LES in predicting a rudimentary landing gear flow with affordable meshes," *International Journal of Heat and Fluid Flow*, vol. 37, pp. 109–122, 2012.
- [83] S. Krajnović, G. Minelli, and B. Basara, "Partially-averaged Navier-Stokes simulations of two bluff body flows," *Applied Mathematics and Computation*, vol. 272, pp. 692–706, 2016.
- [84] S. Krajnović and G. Minelli, *Progress in Hybrid RANS-LES Modelling*, vol. 130 of *Notes on Numerical Fluid Mechanics and Multidisciplinary Design*. Cham: Springer International Publishing, 2015.
- [85] S. Krajnović, G. Minelli, and B. Basara, "Partially-Averaged Navier-Stokes Simulations of Flows Around Generic Vehicle at Yaw," *SAE Technical Paper*, 2016.
- [86] S. Jakirlic, L. Kutej, B. Basara, and C. Tropea, "Computational Vehicle Aerodynamics by Reference to DrivAer Model Configurations," *ATZ worldwide*, vol. 5, pp. 66–72, 2016.
- [87] S. Jakirlic, L. Kutej, P. Unterlechner, and C. Tropea, "Critical Assessment of Some Popular Scale-Resolving Turbulence Models for Vehicle Aerodynamics," *SAE International Journal of Passenger Cars - Mechanical Systems*, vol. 10, no. 1, pp. 2017–01–1532, 2017.
- [88] J. Smagorinsky, "General circulation experiments with the primitive equations," *Monthly weather review*, vol. 91 (3), pp. 99–165, 1963.
- [89] S. Krajnović, "Large eddy simulation of flows around ground vehicles and other bluff bodies.," *Philosophical transactions. Series A, Mathematical, physical, and engineering sciences*, vol. 367, pp. 2917–2930, 2009.
- [90] M. Germano, "Turbulence: the filtering approach," *Journal of Fluid Mechanics*, vol. 238, pp. 325–336, 1992.
- [91] S. S. Girimaji, "Partially-Averaged Navier-Stokes Model for Turbulence: A Reynolds-Averaged Navier-Stokes to Direct Numerical Simulation Bridging Method," *Journal of Applied Mechanics*, vol. 73, no. 3, p. 413, 2006.
- [92] S. Girimaji and K. Abdol-Hamid, "Partially Averaged Navier–Stokes Model for Turbulence: Implementation and Validation," *AIAA paper*, 2005.
- [93] AVL, "Fire manual v2014," 2014.

- [94] D. D. Kosambi, "Statistics in Function Space," *The Journal of the Indian Mathematical Society*, vol. 7, pp. 76–88, 1943.
- [95] J. L. Lumley, "The Structure of Inhomogeneous Turbulent Flows," in *Atmospheric turbulence and radio propagation* (A. M. Yaglom and V. I. Tatarski, eds.), pp. 166–178, Moscow: Nauka, 1967.
- [96] P. Holmes, J. L. Lumley, G. B. Thomson, and C. W. Rowley, "Turbulence, coherent structures, dynamical systems and symmetry," *Cambridge University press*, p. 2500, 1997.
- [97] L. Sirovich, "Turbulence and the dynamics of coherent structures part i: coherent structures," *Quarterly of Applied Mathematics*, vol. XLV, no. 3, pp. 561–571, 1987.
- [98] P. Schmid, "Dynamic mode decomposition of numerical and experimental data," *Journal of Fluid Mechanics*, vol. 656, pp. 5–28, jul 2010.
- [99] P. J. Schmid, L. Li, M. P. Juniper, and O. Pust, "Applications of the dynamic mode decomposition," *Theoretical and Computational Fluid Dynamics*, vol. 25, pp. 249–259, aug 2011.
- [100] J. Tu, C. Rowley, E. Aram, and R. Mittal, "Koopman spectral analysis of separated flow over a finite-thickness flat plate with elliptical leading edge," *AIAA Paper 2011*, no. January, pp. 1–14, 2011.
- [101] J. Östh, B. R. Noack, S. Krajnović, D. Barros, and J. Borée, "On the need for a nonlinear subscale turbulence term in POD models as exemplified for a high Reynolds number flow over an Ahmed body," *Journal of Fluid Mechanics*, pp. 1–26, oct 2013.
- [102] J. Östh, E. Kaiser, S. Krajnović, and B. R. Noack, "Cluster-based reduced-order modelling of the flow in the wake of a high speed train," *Journal of Wind Engineering and Industrial Aerodynamics*, vol. 145, pp. 327–338, 2015.
- [103] T. W. Muld, G. Efraimsson, and D. S. Henningson, "Flow structures around a high-speed train extracted using Proper Orthogonal Decomposition and Dynamic Mode Decomposition," *Computers and Fluids*, vol. 57, pp. 87–97, mar 2012.
- [104] J. L. Lumley, *Stochastic Tools in Turbulence - Applied Mathematics and Mechanics*. New York: Academic Press, 1970.
- [105] D. Rempfer and H. F. Fasel, "Evolution of three-dimensional coherent structures in a flat-plate boundary layer," *Journal of Fluid Mechanics*, vol. 260, p. 351, 1994.
- [106] C. Chovet, M. Lippert, L. Keirsbulck, and J. M. Foucaut, "Dynamic characterization of piezoelectric micro-blowers for separation flow control," *Sensors and Actuators, A: Physical*, vol. 249, pp. 122–130, 2016.